Journal of Energy Storage 161 (2026) 121887

Contents lists available at ScienceDirect

Journal of Energy Storage

journal homepage: www.elsevier.com/locate/est

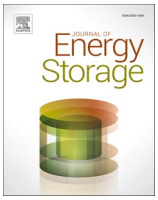

Research Papers

Assessing the critical role of graphite in the carbon footprint of lithium-ion battery production

Pushpendra [a,b,*], Elias Vollert [a,b], Dominic Bresser [a,b,c], Marcel Weil [a,b]

[a] Helmholtz Institute Ulm (HIU), Helmholtzstraße 11, 89081, Ulm, Germany
[b] Karlsruhe Institute of Technology (KIT), 76021, Karlsruhe, Germany
[c] Ulm University (UUlm), 89069, Ulm, Germany

ARTICLE INFO

Keywords:
Life cycle assessment
Carbon footprint
Lithium-ion battery
Synthetic graphite
Natural graphite
Sourcing

ABSTRACT

The central focus of existing life cycle assessment (LCA) studies on lithium-ion battery (LIB) cell production has been around cell manufacturing energy, different cathode chemistries, and the supply chain of cathode active materials. In contrast, the crucial role of graphite as the anode active material on the carbon footprint (CF) of LIB cell production has remained largely underexplored. Particularly the differences between synthetic and natural graphite, and their varying compositions in LIB anodes and sourcing are not considered. This work addresses this gap by conducting an LCA on LIB cell production using latest industrial primary LCA data for both graphite types. The results highlight that the CF of LIB cell production is substantially higher (93 kg CO_2eq. kWh^{-1}) than LIB cell with older graphite datasets (58 kg CO_2eq. kWh^{-1}), with graphite emerging as a key hotspot (37 kg CO_2eq. kWh^{-1}, 26.85 kWh kWh^{-1}). Results show that the choice and proportion of the graphite types in the anode strongly influence the CF of LIB cell production. Furthermore, the findings reveal the importance of relative proportions of the two graphite types in benchmarking where different ratios of graphite types may lead to different benchmarking results. Moreover, the origin of the graphite substantially influences the overall CF of LIB cell production. Utilizing graphite sourced from regions with a higher proportion of renewable energy in their electricity mix significantly reduces the CF of cell production compared to graphite sourced from regions with a lower share of renewables. Nevertheless, the study underscores the importance of including the full life cycle data (use-phase and end-of-life) into future assessments to fully capture the effects of different proportions of the two different graphite types on performance and cycle life for a robust decision making on the optimal ratio of graphite in LIB cell design from an environmental perspective. Overall, the study provides important insights for multiple stakeholders by highlighting the pivotal role of graphite, its types, and sourcing in determining the environmental performance of LIB cell.

1. Introduction

To achieve the European Union's (EU's) ambitious 2040 climate target, a 90% net reduction in greenhouse gas (GHG) emissions compared to 1990, the transport sector, as the leading contributor to GHG emissions in the EU, must be decarbonized significantly [1,2]. To address this, the EU has introduced several laws such as the zero-emission target for new passenger cars and light commercial vehicles, as well as a second emissions trading system (EU ETS II) that puts a carbon price on road transportation [3]. These decisions have led the automotive industry to accelerate the transition to the production of zero-emission vehicles (ZEVs), i.e., battery electric vehicles (BEVs), fuel cell-powered vehicles (FCVs), and other hydrogen-powered vehicles. In this transition BEVs are emerging as the dominant drivetrain technology [2]. In parallel, stationary batteries are playing a critical role in storing excess renewable energy and supporting the broader energy transition [4]. As this shift accelerates, the demand for batteries in the EU for both e-mobility and stationary energy storage is expected to grow significantly from 260 GWh in 2024 to around 1 TWh in 2030 [5]. To ensure that this transition will be both sustainable and competitive, the EU has adopted the Battery Regulation (2023/1542), which aims to establish a safe and sustainable battery value chain [6]. This regulation places particular emphasis on the carbon footprint (CF) of batteries used in electric vehicles, light means of transport, and rechargeable industrial

* Corresponding author at: Karlsruhe Institute of Technology (KIT), 76021, Karlsruhe, Germany.
E-mail address: pushpendra.pushpendra@kit.edu (Pushpendra).

https://doi.org/10.1016/j.est.2026.121887
Received 19 December 2025; Received in revised form 15 February 2026; Accepted 27 March 2026
Available online 2 April 2026

batteries with a capacity exceeding 2 kWh.

Lithium-ion batteries (LIB) are likely to remain the leading battery technology across many applications over the next decade, even if emerging technologies like sodium-ion batteries (SIBs) are slowly entering the market, benefitting from the established supply chains, established production facilities, maturity of technology, decreasing cost and economy of scale [7]. Several life cycle assessment (LCA) studies have been conducted to quantify the environmental footprint (EF) of LIBs throughout their service life [8–14]. These studies have reported that as the share of renewable energy (RE) in the electricity mix increases, the energy intensive battery cell manufacturing stage, which heavily relies on critical raw materials (CRMs) such as cobalt, lithium, and natural graphite, becomes more dominant than the use phase. The battery cell is the fundamental unit of a LIB and typically accounts for 60% to 90% of the total battery weight [15]. Battery cells are integrated into different structural configurations, namely cell-to-module (CTM), cell-to-pack (CTP), cell-to-chassis (CTC), or cell-to-body (CTB), depending on targeted performance metrics, safety requirements, cost constraints, and overall system design objectives, prior to installation in the vehicle architecture [7].

The primary focus of existing LCA studies of battery cell production has been around cell manufacturing, different cathode chemistries, and the supply chain of cathode active materials (CAMs) [10,16–33]. The impacts of anode chemistry and the supply chain of anode active materials (AAMs), which is one of the largest weight shares of battery cell materials making around 15–20% of battery cell mass [34], on the EF of LIB cells have been insufficiently explored in the existing LCA studies. This gap is primarily due to the lack of reliable, primary data on graphite for batteries in major environmental databases such as Ecoinvent, leading researchers to rely on potentially outdated or unrepresentative datasets in their assessments [35]. Currently, graphite either as the only AAM or blended with small shares of nonstoichiometric silicon oxide (SiO_X) or Si accounts for the vast majority, i.e., around 90%, of the anode materials used in LIB, whereas alternative anode materials such as lithium titanate ($Li_4Ti_5O_{12}$, LTO) or silicon-rich anode composites are used to a much lower extent [7,36]. It has been reported that the graphite demand for LIBs in the EU will increase drastically even more than other cathode materials in the upcoming years, implying the critical importance of graphite for the European battery value chain [5,37–39]. Along with the rising demand for graphite, increasing geopolitical uncertainties, trade barriers, and high dependence on foreign producers are driving the global efforts to diversify and strengthen domestic production capabilities to address the supply chain issues for a resilient and sustainable battery-grade (BG) graphite sector [40,41].

BG graphite, in other words, a high-purity graphite (99.95% carbon content by weight), is classified into two types: BG-natural graphite (BG-NG), and BG-synthetic graphite (BG-SG) [35]. In practice, graphite-based anodes in LIB typically use a blend of SG and NG, with the ratio adjusted to balance the performance, safety, and cost based on the specific application [36]. Regarding the LCA of BG graphite, Engels et al. [35] reported that the existing datasets for both BG-SG and -NG are inaccurate, incomplete, outdated, and unrepresentative. As a result, the actual EF of both BG- SG and -NG have been systematically underestimated in the past in LCA studies. In response, several efforts have focused on improving the LCA data quality for both BG-SG and BG-NG by incorporating primary data [36,40,42]. Notably, Engels et al. [40] conducted a cradle-to-gate LCA for a vertically integrated BG-NG production from a Chinese graphite producer and provided transparent, primary life cycle inventory (LCI) data. The reported CF is 9.6 kg CO_2eq. kg^{-1} BG-NG, which is more than four times higher than the reported CF of BG graphite in one often used LCI-database ("*graphite production, battery grade*", Ecoinvent version 3.9.1 and versions before) [43]. Similarly, Carrère et al. [36] presented a LCI for BG-SG via the Acheson powder route, which is the current mainstream production method, based on mainly primary industrial data, and reported a CF of 42.2 CO_2eq. kg^{-1} BG-SG, which is two to ten times higher than previously reported values. These new datasets highlight that earlier LCA studies have underestimated graphite's contribution to the overall EF of LIBs [8,16,17,21,28,29,44,45]. As a result, the critical role of graphite in the total EF of LIB cells has not been explored in details. Furthermore, there has been very little discussion on the choice or different ratios of graphite types in graphite-based anodes and the impact of sourcing the graphite from different regions from an environmental perspective. Consequently, the environmental implications of sourcing and using different types and ratios of graphite in LIB anodes remain largely unaddressed in the current literature. This study aims to first contrast previously published LCA results on LIB cell production with the new LCA datasets for BG graphite, assuming a 50:50 ratio of BG-SG and BG-NG in the AAM. Then, it systematically investigates how varying the proportions of SG and NG in graphite-based anodes and their supply chains influences the overall CF of LIB cells.

The remainder of this paper is structured as follows: Chapter 2 introduces the types of BG graphite, their production pathways, and supply chain, and provides a review of current research on the LCA of BG graphite and LIBs. Chapter 3 describes the LCA methodology, including the goal and scope, LCI data, and system boundaries. Chapter 4 presents the results along with a sensitivity analysis, limitation and directions for future work, and discusses their implications. Finally, Chapter 5 concludes this study.

2. State of research

2.1. BG graphite types and their production process

Graphite is a critical component of LIB anodes, accounting for over 90% of the anode material in commercial applications [7]. BG graphite is typically available in two forms: BG-NG, produced via purification of natural ores, and BG-SG, produced by graphitizing carbon-rich precursors – either petroleum-based or bio-based [35,46–48]. In industrial-scale BG-SG production, the main petroleum-based carbon feedstocks include petroleum coke, tar pitch (coal- or ethylene-based), and needle coke (oil- or coal-based) [48]. More recently, research on the upcycling of bulk plastic waste into BG-SG has shown promising results, although such efforts are currently limited to the lab-scale [49]. In parallel, biochar has attracted growing interest as a bio-based alternative precursor; however, the production of BG bio-graphite is still at an early stage due to its improvable performance in LIBs [46]. Generally, graphite-based anodes for LIBs typically use a mix of BG-NG and BG-SG to optimize both cost and performance; the latter including the achievable reversible capacity, first-cycle capacity loss, and fast charging [36,50,51]. As a result, high-performance applications such as electric vehicles typically employ a higher share of BG-SG, whereas cost-sensitive applications like stationary energy storage and power electronics devices favor a higher proportion of BG-NG [52,53]. In any case, while both types serve the same function of reversibly storing lithium-ions during charge and discharge, they differ significantly in origin, structure, and cost. BG-NG, which tends to be characterized by larger crystals and greater anisotropy, frequently offers slightly higher capacities than BG-SG at the expense of a somewhat short cycle life, especially when subjected to fast charging, and has historically been more cost effective than BG-SG [36,54–57], although continuous efforts are being made to improve the performance of BG-NG for LIBs [58]. However, the cost effectiveness of BG-NG combined with increasing pressures for climate neutrality are expected to boost BG-NG's market share [56,58]. A comparative overview of the key properties of BG-SG, derived from petroleum-based carbon-rich precursors, and BG-NG is presented in Table 1, illustrating the principal distinctions between the two material types. It should be noted, however, that these trends represent general tendencies; both NG and SG exhibit a broad range of characteristics and performance metrics depending on their respective sources, synthesis/mining routes, remaining impurities, crystallinity, and (post-) processing conditions.

Table 1
Comparison of common properties of BG-NG and BG-SG.

Properties	BG-NG	BG-SG
Source of production	Natural ores [36,59]	Petroleum-based precursors [36,59]
Consistency/ morphology	Flaky; less uniform particle size; anisotropic [59,60]	Spherical; rather consistent particle morphology; isotropic [54,60]
Production cost	$6500/t to $7500/t [56]	$7000/t to $8000/t [56]
Supply risk	High, owing to the geographical concentration of NG mining and refining, particularly in China [41,61]	Moderate-to-High, as precursor feedstocks are widely available; however, production and refining remain regionally concentrated [41,61]
Specific capacity	Theoretical capacity of 372 mAh g^{-1}; in practice often close to theoretical value, due to larger grain sizes[a] [54,61–64]	Theoretical capacity of 372 mAh g^{-1}, typically slightly lower in practice due to smaller grain sizes[a] [54,61–64]
Thermal stability and safety	Moderate to low (natural impurities, structural defects) [54,65]	Relatively high (low impurity levels, structural uniformity) [54,65,66]
Tap density	Around 1.0–1.2 g cm^{-3} (dependent on particle size, shape, surface texture) [67–69]	Around 1.0–1.2 g cm^{-3} (dependent on particle size, shape, surface texture) [67–69]
Cycle life	Relatively higher capacity fade during long-term cycling [58,70,71]	Frequently, higher cycling stability and capacity retention [58,70,71]
Performance in LIBs	Moderate rate capability; higher irreversible capacity losses [54,72]	Commonly, greater rate performance [54]

[a] As other factors such as crystallinity, particle size, surface area, and purity strongly influence the specific capacity and vary within both NG and SG, a clear distinction between the two is difficult to draw.

NG is typically classified into three types, i.e., amorphous, flake, and lump or vein, based on its crystallinity, particle size, morphology, and the location of its deposits [73]. Among these, flake-type graphite is the most commonly used material for LIB anodes [74]. BG-NG is produced from flake graphite ore via the following processes: mining, separation, spheroidization, purification, and surface coating [35,36,40,42]. Initially, the NG ore is mined in either open-pit or underground. In next step, mined ore is separated from the rock and other minerals via crushing, milling, and flotation, resulting into a wet carbon concentrate. After flotation, the wet carbon concentrate is filtered, dried, and depending on its particle size distribution screened into two fractions: small flakes and powders suitable for the spherical graphite and large flakes suitable for different applications (e.g. graphite foils) [40]. Subsequently, the small flakes and powder undergoes a milling technique called spheroidization to achieve potato-shaped graphite particles with sizes of approximately 10–20 μm for an improved electrode density, fast charging capabilities, and a more uniform intercalation of lithium ions [75,76]. Typically, the spheroidization process is carried out by using multiple classifier mills in a row in order to carefully first micronize and afterwards to spheroidize the flake graphite particles step by step [40]. To increase the carbon content to more than 99.95% and remove the various impurities such as calcium, aluminum, silicon, and chromium from spherical graphite, spherical graphite particles are further purified. In the last step, purified spherical graphite (PSG) particles get coated with a thin layer of carbon to enhance electronic conductivity, reduce particle degradation and improve the initial Coulombic efficiency. These steps yield commercially available BG-NG anode materials [54,77,78]. A more detailed description of the BG-NG production process is provided in a paper by Engels et al. [40].

SG is artificially produced from carbon-rich precursors. Industrial-scale BG-SG production from petroleum-based carbon feedstocks involves three main stages: pre-treatment, material processing, and particle refinement [35,36]. In the first step of BG-SG production, the precursor is converted into soft carbon through thermal treatment at 800–1200 °C [35]. In the next stage, the soft carbon is subjected to milling, being crushed, grinded, and eventually classified into a particle size at the mm scale [35]. The classified milled precursor is then graphitized at over 2500 °C, inducing the structural rearrangement of carbon atoms into an ordered graphite lattice [35]. Graphitization can be performed via three different commercial routes: the Acheson powder route, Acheson block route, and length-wise graphitization (LWG) block route, having significant differences in consumable material consumption and energy efficiencies [36]. The Acheson powder route is currently the state-of-the-art commercial production route for producing BG-SG [36]. In the last stage of particle refinement, the graphitized powder is reduced to a size of 10–20 μm in a process called micronizing and a carbon coating is applied on the surface of the micronized graphitized powder to achieve the BG-SG anode material. For further details on the BG-SG production process, see Carrère et al. [36]. A general overview of stages for both BG-NG and -SG is provided in Fig. 1.

2.2. *Global distribution of graphite production and EU's strategic projects on BG graphite*

China continues to dominate the global supply chain of BG graphite, currently producing over 92% of the global supply [56,79]. In 2021, more than 70% of global NG ore production originated from China, mainly in the northern and eastern provinces of Heilongjiang, Inner Mongolia, and Shandong [52,80,81]. The remaining global share of NG ore was spread across Brazil (~7%), Mozambique (~3%), Russia (~2.5%), Madagascar (~2%), and other smaller producers [81,82], while Mexico and Norway are rising investors in mine production [83]. More critically, China continues to dominate the downstream processing stage, producing approximately 99.6% of the world's PSG, the key precursor for LIB anodes, in 2020 [84]. Due to this high concentration, combined with the strategic importance of NG in industries such as batteries, steel, aerospace, defence, and drones, NG has been included in the EU's CRM list since its second edition in 2014 [85].

While SG presents a comparatively lower supply chain risk than NG, it too remains heavily influenced by Chinese production capacities responsible for up to 56% of world's SG [52]. The remaining global share of SG is spread across producers in North America (United States, Mexico, and Canada), Europe, Japan, South Korea, and Sub-Saharan Africa with smaller start-ups, investment projects, and firms [86]. Similar to NG, the major SG processing facilities are based in China's eastern and northern provinces, which together accounted for around 57% of the country's total SG production in 2023 [87]. However, amid China's climate neutrality push, several leading SG producers such as Yunnan Shanshan Co. Ltd. and Ningbo Shanshan Co. Ltd. have announced plans to build and expand the SG production facilities in the southwest region to leverage the region's excess renewable energy [87,88]. Once these announced capacities materialise, the northern and eastern region's share of China's total SG production is expected to decrease to 31%, while the southwest region's share is projected to rise to around 35%. Considering SG's supply vulnerability and role as an NG alternative in critical sectors, EU's Critical Raw Material Act (CRMA) has recently identified SG as a CRM. Consequently, both NG and SG are now formally recognized as CRMs within the EU framework [52,89]. To further strengthen supply security and strategic autonomy, the CRMA also designates certain materials as Strategic Raw Materials (SRMs). Within this framework, BG graphite, including both BG-NG and BG-SG, has been officially recognized as an SRM. Of the 60 strategic projects supported under the CRMA, 14 (10 within the EU and 4 internationally) specifically focus on the extraction, processing, substitution, or recycling of BG graphite (Table 2), reflecting the EU's targeted efforts to address supply chain vulnerabilities for BG graphite [90,91].

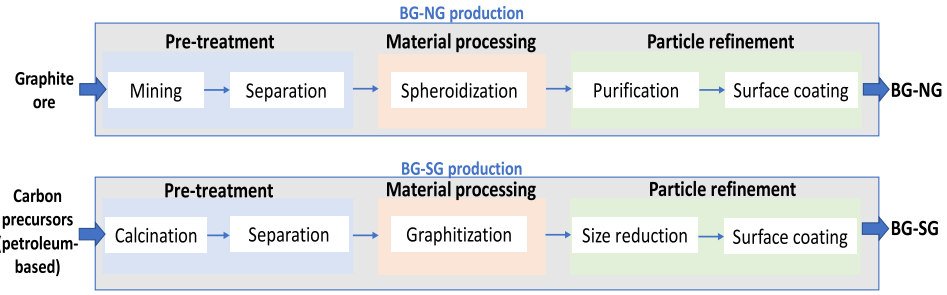

Fig. 1. General overview of production stages for BG-NG and BG-SG (based on Engels et al. [35], Engels et al. [40], and Carrère et al. [36]).

Table 2
List of strategic projects for BG graphite under EU's CRMA [90,91].

Sr. nr.	Project name	Type	Promoter	Country	Production start in (estimated)	Capacity (designed/announced) (in tonnes per annum (tpa))
1	SALROM Baia de Fier	Extraction	Societatea Națională a Sării S.A.	Romania	2027	15,000 tpa [92]
2	Talga Natural Graphite ONE	Extraction	Talga AB	Sweden	2027	~100,000 tpa [93]
3	Greenland Graphite a/s and norgraph a/s	Integrated: Extraction and processing	GreenRoc Strategic Materials Plc	Greenland and Norway	No information	~80,000 (concentrate) tpa [94]
4	Maniry Graphite Mine Project	Extraction	Evion Group NL	Madagascar	2025	39,000 (concentrate) tpa (stage one), scaling to 56,400 (concentrate) tpa (stage two) [95]
5	Sarytogan Graphite Project	Extraction	Sarytogan Graphite Limited	Kazakhstan	2027	~50,000 (concentrate) tpa [96]
6	Balakhivka Graphite Deposit	Extraction	Pobuzhzhya's Development LLC	Ukraine	2028	38,000 tpa [97]
7	BAM4EVER (Phase I + II)	Processing	Tokai COBEX savoie	France	2026	50,000 tpa by 2030 [98]
8	CO2Graphite	Processing	UP Catalyst	Estonia	2025	60,000 (carbon materials) tpa by 2030 [99]
9	European Initiative for Strategic and Sustainable Graphite Production	Processing	NGC Battery Materials GmbH	France (main location), Namibia, Germany	2028	20,000 tpa by 2028, with potential scale up to 50,000 tpa [100]
10	GALLICAM	Processing	Sibanye-stillwater Sandouville Refinery	France	2027	No designed tpa mentioned
11	Hycamite TCD Technologies Ltd	Processing	Hycamite TCD Technologies Ltd.	Finland	No information	6000 (high quality carbon) tpa [101]
12	Hydrometallurgy	Recycling	ORANO Batteries	France	2030	No designed tpa mentioned
13	NorthCYCLE	Recycling	Northvolt Revolt AB	Sweden	No information	No designed tpa mentioned
14	ProHiPerSi	Substitution	PCC Thorion GmbH	Germany	2029	No designed tpa mentioned

2.3. LCA of BG-NG and BG-SG and their incorporation in databases

One of the first LCAs on NG was conducted by Pehnt in 2002 [102]. It looked at the full production chain from mining in Zimbabwe to processing in Germany, and used data for material and energy consumption from Graphitwerk Kropfmühl AG. The study estimated a combined energy use of 15 kWh and 13.5 kg CO_2eq. kg^{-1} of NG production. It is worth noting that the NG in this case was used for fuel cells, not batteries. Nevertheless, the results were widely accepted and used in the Sphera database (also known as GaBi) until 2020 [40]. This database is commonly used by OEMs such as Audi, BMW, Daimler, and VW, as well as by the chemical industry [40].

In 2020, Sphera updated the NG database based on studies from Zhang et al. [103] and Gao et al. [104]. Both studies covered BG-NG production stages from mining, beneficiation, purification, and surface coating and derived their LCI data mainly from published literature, engineering calculations, manufacturing manuals, and Chinese national production standards. Both studies provided only aggregated LCI data for the entire process and reported direct process-related emissions of 7.75 kg CO_2eq. kg^{-1} BG-NG and 5.25 kg CO_2eq. kg^{-1} BG-NG, respectively. Engels et al. [35] reported several inconsistencies regarding data collection, data origin and quality, and the assumptions made in both studies. One such inconsistency identified by Engels et al. [35] is that the reported CF of 5.3 kg CO_2eq. kg^{-1} of BG-NG in Geo et al. [104] seems very low when considering the additional expenditure for electricity, diesel, coal, etc.

Recently, Engels et al. [40] provided a more detailed LCI for BG-NG production based on industrial primary data from a Chinese graphite producer. The authors provided comprehensive LCIs for each step of BG-NG production process- including mining, separation, spheroidization, purification, and surface coating. All stages, except spheroidization (which generated graphite fines as a co-product) were single-output processes. The spheroidization process achieved a yield of about 40%, resulting in 60% of the input being produced as a byproduct in the form of graphite fines. The LCA results reported a total energy requirement of approximately 11 kWh kg^{-1} and CF of 9.6 kg CO_2eq. kg^{-1} of BG-NG produced, and identified the coating stage as the primary hotspot, accounting for around 4.5 kWh kg^{-1} BG-NG.

In recent years, several graphite producers have started disclosing the CF for their BG graphite. For example, Nouveau Monde Graphite Inc. (NMG), a NG producer based in Quebec, Canada, hired an LCA consultancy (Minviro) to conduct the LCA of their product [105]. The LCA covered the entire process from extraction of NG ore to final processing. The complete process chain for their BG-NG production is based in Quebec, where electricity is largely sourced to approx. 94% from hydropower [106]. They reported a CF of 1.23 kg CO_2eq. kg^{-1} BG-NG, and attributed this comparatively low value to the use of their proprietary thermochemical purification technology, replacing conventional acid

leaching, and the implementation of all-electric processes from mining to final production. Similarly, Talga Group Ltd., a battery anode material producer based in Sweden, provided a cradle-to-gate LCA, conducted by Minviro, for their flagship anode product, Talnode®-C [107]. The assessed stages from mining to BG-NG production are all located in Sweden, and the reported CF is 1.7 kg CO_2eq. kg^{-1} BG-NG. The company attributed this low CF to the use of high-grade NG ore, 100% Swedish renewable hydropower, and their proprietary anode production technology.

Among the existing LCA literature on BG-NG production, the peer reviewed study from Engels et al. [40] stands out for providing high-quality LCI data that are representative, disaggregated to the process level, and based on primary industrial data. The findings from this study have been integrated into major LCA databases, including GREET (versions from 2022 onwards), the latest Ecoinvent release ("*coated natural graphite production*", V 3.11, 2024,), and Sphera ("*Natural graphite anode powder (for use in LIB)*", 2024) for BG-NG production, and hence used as a reference for BG-NG in this study [55,108,109].

Notter et al. [44] modelled SG production by NG mining and further thermal processing to represent the production of 1 kg of SG. A total energy consumption of around 1.05 kWh kg^{-1} of BG graphite is reported in the LCI. Although the study did not consider the complete process chain for BG graphite production (excluded downstream processing steps such as coating) and process yield, which probably led to a significant underestimation of the energy consumption [40]. Due to the lack of primary data for several processes, Notter's LCI was based on several assumptions, and thermodynamic calculations, as discussed in detail by Engels et al. [40]. Despite of this, Notter's LCI was used to represent both BG-NG and BG-SG production in Ecoinvent till V 3.7.1 (2020) [110].

Dunn et al. [111] from the Argonne National Laboratory in the USA presented an LCI for the SG production. The stages included in the production of SG were the grinding of petroleum coke, mixing with coal tar pitch, extrusion, baking and graphitization via the Acheson block route. Like Notter et al. [44], the authors also did not include the material and energy consumption for the last stage of the particle refinement for yielding BG-SG. The authors estimated the energy requirements for baking and graphitization from their own estimates and thermodynamic calculations without presenting clear data sources and reported a combined energy requirement of 6.1 kWh kg^{-1} of BG-SG for both processes. Both Ecoinvent ("*synthetic graphite production, battery grade*", V 3.8-3.10.1) and GREET (versions prior 2022) used this study as a reference for BG-SG production [55,112].

A more detailed LCI based on publicly available data is reported by Surovtseva et al. [42]. Their study provided detailed material and energy flows, as well as emissions, for several BG-SG production stages. The study considered the Acheson block route for graphitization, citing an energy demand of 0.9 kWh kg^{-1} BG-SG from Dunn et al. [111]. However, Dunn et al. [111] reported 4.5 kWh kg^{-1} BG-SG for this process. Consequently, this discrepancy – whether due to a citation error or differing assumptions – remains unexplained. However, a combined energy demand of 8.8 kWh kg^{-1} BG-SG for the thermal treatment, baking, and graphitization processes, and a total energy demand of 12.75 kWh kg^{-1} BG-SG for the complete process chain (including the energy for the production of green coke and tar pitch) was reported in the LCI.

Iyer and Kelly [55] presented an updated LCI of Dunn et al. [111], incorporating the LCI data for the stages of thermally converting green coke into needle coke and baking from Surovtseva et al. [42], while making specific modifications based on other references, as necessary. Daimer [113] indicated that Acheson furnaces have been continuously replaced by LWG furnaces over the past few years owing to their higher energy efficiency, lower cost owing to smaller furnace sizes, and improved homogeneity in their final product. Hence, the authors assumed the LWG furnace for the graphitization process and the data about the energy consumption (2–3 kWh kg^{-1} BG-SG) of this process were taken from Daimer [113]. The LCI indicated a combined energy demand of approximately 10 kWh kg^{-1} BG-SG for the calcination, baking, and graphitization processes and the findings from this study were integrated in GREET (versions from 2022 onwards) for BG-SG [55].

In the LCIs from the abovementioned studies, the complete process chain for the Acheson block route and the main processes for the particle refinement stage, such as micronizing and coating, were not considered extensively. Sphera (2023) used a mix of several publicly available sources and independently collected primary industrial data to build a complete LCI for the BG-SG production ("*Synthetic graphite anode powder (block route), for use in LIB*") [36]. It considered all process steps associated with the Acheson block route, i.e., the milling of the calcined coke and the block forming prior to the block baking process, and also included the micronizing and coating processes from the final stage of the BG-SG production. The reported energy consumption for the baking and graphitization processes were 11 and 8.57 kWh kg^{-1} of BG-SG, respectively. In all the aforementioned studies, the LCIs were not entirely derived from primary industrial data, and often neglected the process yields and auxiliary materials (graphite crucible and packing media) in processes such as the baking and graphitization. Additionally, most studies focused on graphitization using the Acheson block method, which is commonly employed to produce graphite for various applications, indeed, but is rarely used for BG graphite used in LIBs [36].

Epsilon Advanced Materials Pvt. Ltd., a multinational BG-SG producer, reported the CF of BG-SG from both its operating and planned production facilities in India, Finland, and the USA in their sustainability report 2023–24 [114]. The LCA, carried out by Minviro, was based on the Acheson powder route for the graphitization, using a pitch-based raw material. The energy consumption of 13 kWh kg^{-1} of BG-SG for the graphitization and a crucible consumption of 0.27 kg kg^{-1} of BG-SG were considered [36]. For the Indian plant, the report mentioned that primary data on mass balance and credits for waste energy utilization were considered, whereas for the planed facility in Finland, the study utilized primary data from company's detailed mass balance projections. The reported CF were 5.2, 4.7, and 8.7 CO_2eq. kg^{-1} BG-SG for the facilities in India, Finland, and the USA, respectively [114]. Similarly, Vianode, an SG producer based in Norway, recently announced the development of a novel closed-furnace technology that outperforms conventional open Acheson furnaces [115]. This process is notably described as highly resource-efficient, with reduced direct emissions, and lower consumption of energy, raw materials, and consumables. An LCA conducted by Minviro estimated a CF of only 1.9 kg CO_2eq. kg^{-1} BG-SG, which is the lowest reported to date. Contributing factors cited for having such a low CF include electricity mix, which is 99% renewables, high material recovery rates, and a very energy-efficient graphitization process.

Recently, Carrère et al. [36] conducted a cradle-to-gate LCA of the BG-SG production, based mainly on primary industrial data for the Acheson powder route, i.e., the mainstream production route for BG-SG. The assessment covered milling (separation), graphitization, micronizing (size reduction), coating, and packaging stages, each with reported process yields. Notably, the authors highlighted that the Acheson powder route does not require the baking step. Calcined coke and coal tar pitch served as main feedstocks, with graphite crucibles and packing media used as auxiliary materials in the graphitization stage. Several by-products were reported at different process stages such as coke fines from milling, used graphite crucibles, SG block machining chips and packing media from graphitization, and graphite fines from micronizing. The graphitization was identified as the most carbon-intensive stage with the electricity use for the graphitization (16 kWh kg^{-1} BG-SG) and graphite crucibles accounting for approximately 46% and 28% of the total CF (42.2 kg CO_2eq. kg^{-1} BG-SG), respectively. The micronizing step, i.e., the second most energy intensive process with a process yield of only 60%, was found to significantly influence upstream stages (graphitization and milling) and was thus highlighted as a crucial step contributing to the overall CF of the BG-SG production. Based on these

new findings, the authors highlighted that the previous studies [44,55,111] used in different environmental databases have significantly underestimated the CF of BG-SG production. The new findings from this study for the BG-SG production have now been incorporated in the latest version of Sphera ("*Synthetic graphite anode powder (powder route)*", 2024), Ecoinvent V 3.11 ("*Synthetic graphite production, battery grade, via Acheson powder route*", 2024), and the GREET (2025) [109,116–118]. The inclusion of this study in these widely used databases indicates that the results are considered as reliable and representative of current BG-SG production pathways.

Wang et al. [48] reported the CF for 12 operational and 22 upcoming SG production facilities in China. Alongside the conventional precursors, i.e., petroleum coke and coal tar pitch, the study also considered oil-based needle coke, coal-based needle coke, and ethylene tar pitch. The authors reported that the feedstock for the BG-SG production varies across facilities, with some utilizing a single precursor, while others employ blends of multiple precursors. The reported plant-specific CF ranged from 6.8 to 12.9 kg CO_2eq. kg^{-1} BG-SG, with variations attributed mainly to differences in feedstock composition and energy efficiency [48]. The authors also briefly discussed the reasons for the large difference in CF between their study and that of Carrère et al. [36]. They attributed their lower CF mainly to lower energy requirements of the graphitizing process (8–13 kWh kg^{-1} BG-SG) and the graphite crucible production, as well as to higher process efficiencies relative to Carrère et al. [36]. However, in the absence of detailed process-level disaggregated LCIs and the lack of transparency on the databases used for background processes, a direct comparison with Carrère et al. [36] remains challenging. For instance, the reported CF of 0.59 kg CO_2eq. kWh^{-1} for the Chinese electricity mix is significantly lower than the values reported in Ecoinvent V 3.10 and 3.11. A comparison of the CF for both BG-NG and BG-SG from various LCA studies (serving as a basis for different environmental databases, see Fig. 3) and graphite producer reports, relative to the lowest CF reported for each BG graphite type, is shown in Fig. 2.

In conclusion, most of the LCA literature on both BG-NG and BG-SG shows considerable variation in data quality, completeness, transparency, and the eventual CF values. Many studies relied on secondary data, covered only partial process chains, and/or used routes that are not representative of actual industrial practices. Furthermore, the limited transparency and absence of disaggregated LCIs in LCA reports from BG graphite producers such as Vianode and Epsilon Advanced Materials Pvt. Ltd. hinder a direct comparison of their processes in terms of energy use, emissions, yields, wastes, and consumables with other studies as the ones by Carrère et al. [36] and Engels et al. [40]. By contrast, Carrère et al. [36] and Engels et al. [40] addressed these issues by providing detailed and process-level LCIs based on primary industrial data for BG-SG and BG-NG. Due to their high data quality and inclusion in the latest versions of widely used environmental databases such as Sphera, Ecoinvent, and GREET, these studies are representative of current BG graphite production pathways and therefore serve as the basis for modelling graphite-based anodes in this study.

2.4. Usage of graphite's LCA in LIBs

Many LIB-related LCA studies [16,19,28,45,119–122] have used the environmental data for BG graphite from Ecoinvent V 3.7.1 or prior, which was based on Notter et al. [44]. Similarly, several U.S.-based LCA studies [17,21,123,124] relied on BG-SG data from the GREET model, derived from Dunn et al. [111]. This study was later incorporated also in Ecoinvent V 3.8 for BG-SG, and used by Abdelbaky et al. [125] alongside BG-NG data from Engels et al. [40]. More recently, Voß et al. [126] applied a different LCI modelling approach for both BG-NG and BG-SG, drawing mainly on datasets from Engels et al. [40] and Carrère et al. [36]. However, several production stages from the source studies [36,40] were omitted in their LCIs modelling to maintain comparability with SIB materials, for which equivalent data were unavailable. While this rationale is understandable, the omissions introduce a bias from an LCA perspective, by excluding key processes such as coating in BG-NG and micronizing in BG-SG, leading to a significantly underestimated CF (a more detailed explanation is provided in the Supplementary Information (SI)).

The interlinkages between the foundational source studies, their inclusion in different versions of different environmental databases, and their subsequent use in LCA research are illustrated in Fig. 3. However, most existing LCA studies on LIBs rely on environmental data for BG graphite from databases or LCA studies that are not fully representative, are based on secondary data, or consider incomplete process chains for both BG-SG and BG-NG, as discussed in the previous section. As a result, these LCA studies tend to underestimate the true contribution of graphite to the overall CF of LIBs. Additionally, existing LCAs and

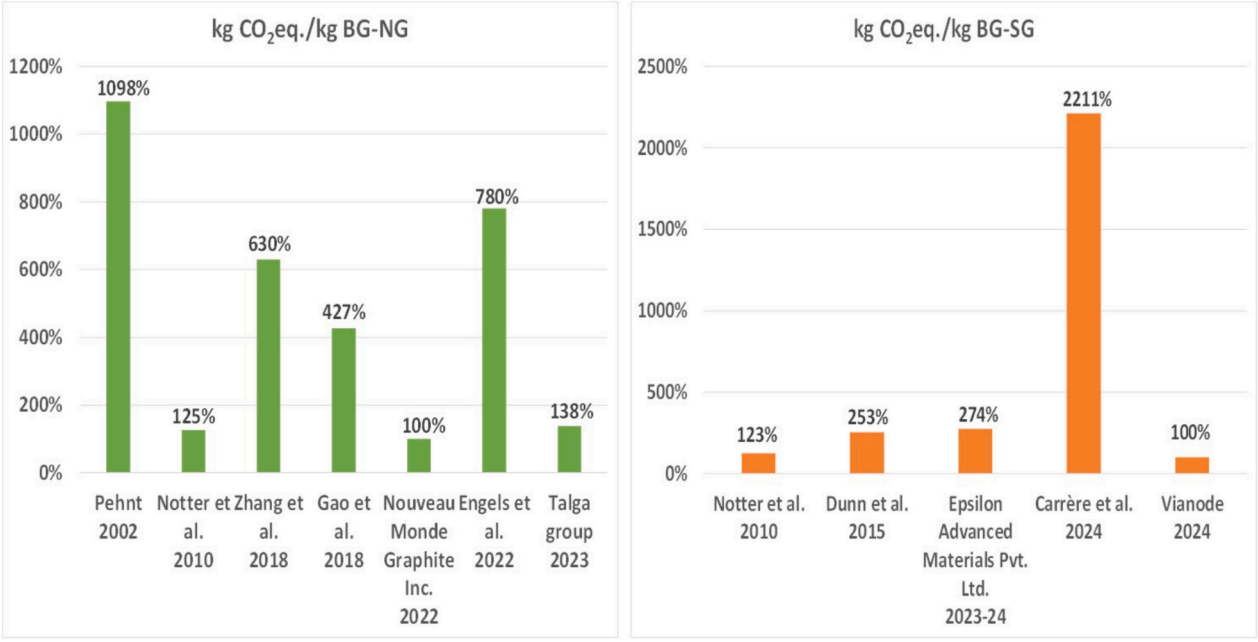

Fig. 2. Comparison of CF of BG-NG (left) and BG-SG (right), relative to the lowest CF reported for each BG graphite type.

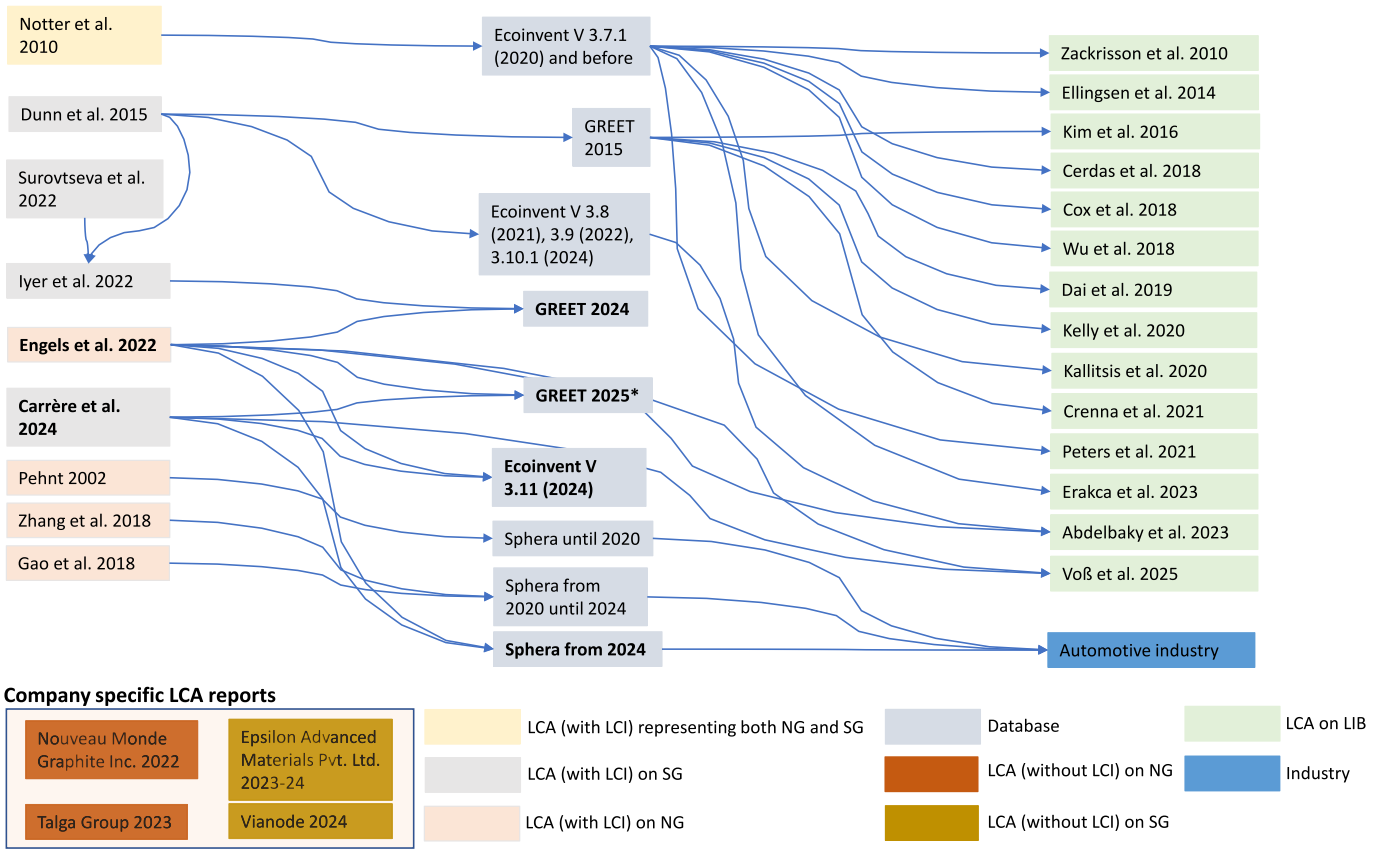

Fig. 3. Top: Overview of LCI sources for BG graphite on the left side, their implementation in environmental databases in the middle, and the usage of different databases for BG graphite in different LCA of LIB on the right. Bottom: company specific LCAs on BG graphite in the box. Schematic representation inspired by Engels et al. [40].

market analyses indicate a broad range in the proportion of BG-SG relative to BG-NG in LIB anodes, with the BG-SG shares varying from 25% up to 90% [36,125–127]. For example, Voß et al. [126] adopted a 75% SG share in LIB anodes for their baseline scenario serving as benchmark for their studies on SIBs, whereas Sprengelmeyer et al. [127] applied a 25% SG share for a similar comparison. Building on recent LCA studies by Engels et al. [40] and Carrère et al. [36], which highlight significant differences in the environmental impacts of BG-NG and BG-SG, and the reported wide variation in their relative shares within LIB anodes, this study addresses the following research question: How do the choice or mix of graphite types with their varying SG-to-NG ratios influence the environmental performance of LIBs? To answer this question, the following chapter presents a cradle-to-gate LCA of LIB cell production using graphite datasets based on Engels et al. [40] and Carrère et al. [36].

* The GREET (2025) model has two production pathways for BG-SG. One pathway follows Pandey et al. [116], with production stages as well as material and energy inputs derived from Carrère et al. [36], while the other pathway is based on Wang et al. [48].

3. LCA of LIB cell production

3.1. Goal and scope

The primary goal of this study is to perform an attributional LCA of the LIB cell production using new environmental datasets for BG-SG [36] and BG-NG [40]. In addition, this study aims to investigate the environmental implications of the choice and varying ratios of the two different kinds of graphite in the anode on the CF of the LIB cell production. The outcomes of this study are expected to challenge previously reported CF values associated with LIB cell production, and shall enable the stakeholders such as battery manufacturers, recyclers, LCA practitioners, and policymakers in making informed decisions from an environmental perspective. Consequently, the results of this study are of high relevance to industry, academia, and policymakers.

The investigated LIB cell is a pouch cell weighing 650.5 g with a specific energy of 225.2 Wh kg^{-1} [20]. For the baseline scenario, the cell uses lithium nickel manganese cobalt oxide ($LiNi_{0.6}Mn_{0.2}Co_{0.2}O_2$, NMC_{622}) as the cathode-active material (CAM), graphite as the anode active material (AAM), polyethylene and polypropylene membranes as the separator, and 1 M $LiPF_6$ in ethylene carbonate (EC) and dimethyl carbonate (DMC) (1:1 by weight) + 2 wt% vinylene carbonate (VC) as the electrolyte, with cell dimensions of 115 mm × 330 mm × 7 mm [20]. The functional unit is 1 kWh of cell energy that translates into a reference flow of 4.44 kg of LIB cell. A sensitivity analysis is performed on the ratio of the different graphite types in the anode, the efficiency of the BG-SG production, the cell specific energy, and the electricity mix for the graphite production.

In line with Erakca et al. [19], an extension of the boundary system to the pack level is considered to investigate the impacts of the results also at the pack level. In addition to the baseline scenario focusing on NMC_{622} as the CAM, a supplementary model incorporating lithium iron phosphate ($LiFePO_4$, LFP) containing LIB cells is developed to improve the representativeness of the study. The outcomes from both chemistries are compared against existing literature to contextualize the findings.

3.2. System boundary

A cradle-to-gate LCA is performed, encompassing the upstream extraction and processing of precursors materials, as well as the cell

manufacturing. The use phase and EoL treatment are excluded from the system boundary, as these life cycle stages have already been studied in Peters et al. [122].

The cell production process is based on von Drachenfels et al. [20]. It starts with the electrode production stage, where initially anode and cathode slurry are prepared by mixing of active materials in individual production lines. Anode and cathode slurries are then coated onto a copper foil and an aluminum foil, respectively, followed by drying. The dried electrodes are then conditioned in a calendaring process before entering the slitting stage that produces electrode coils. The electrode coils are then further dried intensively in a vacuum oven in intensive drying stage, concluding the electrode production stage. The intensive drying stage is directly connected to the cell assembly stage, which takes place in a dry room with dew point of −40 °C. Initially, the anode and cathode coils are separated into individual sheets using a laser cutting process, after which the electrode sheets are assembled with separators through a high-speed stacking process. In the following stage, electrodes are contacted and connected with tabs using a laser welding process. In the final assembly, the cell stacks are packed in the pouch bag, after which the electrolyte is filled under vacuum, and the pouch bag is subsequently sealed. In the final stage of cell production, i.e., the cell finishing, the cell is pre-cycled to enable the formation of the solid electrolyte interphase (SEI), which generates gases that are subsequently removed through a degassing step [128]. Later testing and aging processes conclude the cell production, where the quality control is performed and various quality parameters are measured. A global average scrap rate of 7.7% at the industrial scale is assumed [129]. The cell production facility is located in Germany and more detailed information on the cell manufacturing process and technical parameters can be found in von Drachenfels et al. [20]. A graphical representation of the system boundaries considered for this study is shown in Fig. 4. As stated earlier, examining the battery pack necessitates broadening the system boundaries to incorporate the assembly process and extra pack components, which is explained in detail in Section 4.3.

3.3. LCI, data sources, and modelling

Material and energy consumption data for the LIB cell production is based on von Drachenfels et al. [20] and provided in Table 3. Their adoption in recent Ecoinvent database releases (V 3.11 and V 3.12) for the energy and heat consumption increases the representativeness of these data for battery production. The LCIs for the battery materials are extracted from Peters and Weil [130], where the authors extracted LCIs for different battery materials from various sources. More specifically, the authors extracted LCIs for NMC_{622}, Al and Cu tabs, and pouch housing from Ellingsen et al. [16], whereas the LCI for polyvinylidene fluoride (PVDF) is based on the study reported by Zackrisson et al. [28]. The study reported by Majeau-Bettez et al. [29] is used to extract the LCI for the separator.

Background data on energy, materials, pre-chain processes, and emissions is used from Ecoinvent V 3.10 (cut-off, unit processes). Open LCA V 2.4.0 software is used for the LCA modelling. ILCD 2011 Midpoint+ is chosen for the life cycle impact assessment (LCIA) method and the considered impact category is climate change. An additional analysis of other impact categories from the chosen LCIA method is provided in the SI.

In order to see the influence of new graphite datasets on the overall CF of the LIB cell production, a comparison of the CF of the LIB cell production with von Drachenfels et al. [20] is made. For this, a reference scenario is made with the same LCI as used for the baseline scenario, but for the former the old graphite dataset ("*graphite production, battery grade | Cutoff, U – CN*", Ecoinvent V 3.10) is used instead of new graphite datasets. While for the baseline scenario, the anode composition in the LIB cell is assumed to consist of a 50:50 ratio of BG-SG and BG-NG. The LCIs for BG-SG and BG-NG are based on Carrère et al. [36] and Engels et al. [40], respectively. Since, the BG-SG production process has multiple valuable by-products, the economic allocation of by-products is considered and the corresponding inputs for the BG-SG production after the economic allocation are taken from Ecoinvent's ecoQuery V 3.11-cutoff. For BG-NG, a conservative approach for the allocation (allocation of all burdens to the final output product) is considered, adopting the same approach followed in the original paper from Engels et al. [40].

Considering the high concentration of both types of BG graphite production in the northern, eastern, and southwest regions of China (Heilongjiang, inner Mongolia, Shandong, Yunnan), the electricity dataset covering this region ("*market for electricity, medium voltage | Cutoff, U-CN-SGCC*" representing time-period 2020–23) is considered for the graphite production [131]. As the cell production is based in Germany, the dataset on electricity and heat are from Germany and Europe without Switzerland, respectively. Electricity datasets for Europe ("*market group for electricity, medium voltage | Cutoff, U- RER*" representing time-period 2015–23), North America ("*market group for electricity, medium voltage | Cutoff, U-RNA*", representing time-period 2015–23), and Northeast grid of China ("*market for electricity, medium voltage | Cutoff, U-CN-NECG*", representing time-period 2021–23) are considered for the BG graphite production in different regions in Section 4.2.3. Transportation and storage are not considered in the study, since their contribution to the overall CF of the cell production has been reported to be negligible [122,130].

For the LFP-based LIB cell modelling, the battery cell components share and the LCI for LFP is based on Peters and Weil [130], where the authors extracted the LCIs for the LFP cathode material and the component share distribution from Zackrisson et al. [28]. For the other battery materials, the LCIs are the same as for the baseline scenario. The

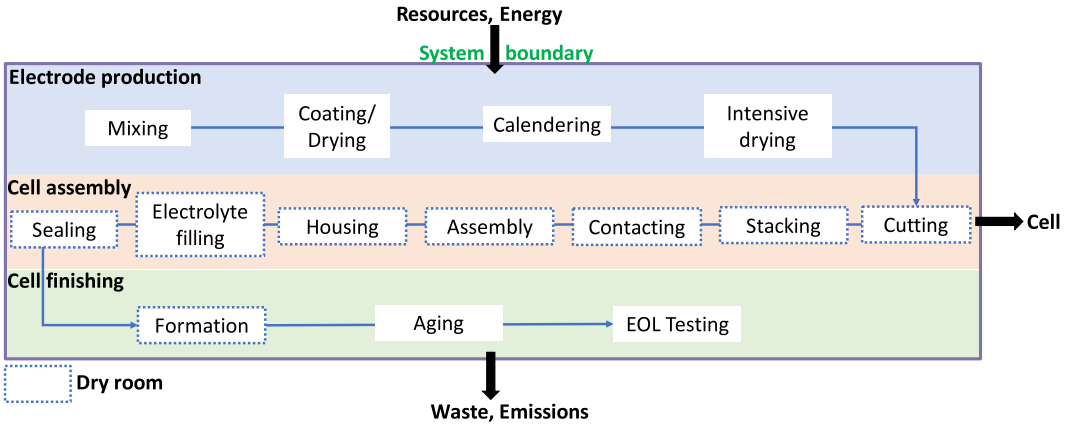

Fig. 4. System boundary and considered production steps in LIB cell production, based on the study by von Drachenfels et al. [20], with the schematic representation inspired by Erakca et al. [19].

Table 3
Material and energy consumption data for cell production processes at each cell production stages (electrode production, cell assembly, cell finishing and environment) and material weight distribution for 1 kg of the NMC_{622}-based LIB cell production (based on von Drachenfels et al. [20]).

Cell production stage	Cell production process	Material (g kg^{-1} cell)		Electricity consumption (Wh kg^{-1} cell)	Gas consumption (Wh kg^{-1} cell)	Material weight (%) distribution in cell
Anode production	Dry and wet mixing	Graphite	244.09	19.35		34.0%
		PVDF	6.30			
		Carbon black	2.46			
		Water	126.42			
	Coating and drying	Copper foil	87.25	125.50	1380.03	
	Calendaring			50.23		
	Slitting			14.13		
	Intensive drying			9.22	387.10	
	Cutting			1.23		
Cathode production	Dry and wet mixing	NMC_{622}	378.34	17.97		43.5%
		PVDF	9.98			
		C65	9.98			
		NMP	159.29			
	Coating and drying	Aluminum foil	36.56	117.82	1295.39	
	Calendaring			47.16		
	Slitting			13.21		
	Intensive drying			8.60	363.44	
	Cutting			1.23		
Cell assembly	Stacking	Separator	18.43	56.84		1.8%
	Contacting	Tabs	1.38	8.60		0.1%
	Assembly			8.60		
	Housing	Pouch foil	46.54	8.60		4.7%
	Electrolyte filling	Electrolyte	157.76	170.66		15.8%
	Sealing			6.45		
Cell finishing	Formation			2232.41	55.76	
	Aging				89.25	
	Testing			223.20		
Environment	Dry room			513.52		
	Total		1000	3654.53	3570.97	100%

specific energy of the LFP-based LIB cell is 160 Wh kg^{-1} [132]. The modelling for the extension of the system boundaries to the pack level is discussed in detail in Section 4.3. Detailed LCIs for the baseline scenario as well as other models used in this study can be found in the SI.

4. Results and discussion

This chapter presents and discusses the results of this study. The analysis begins with a comparison of the CF between the baseline and the reference scenario for the LIB cell production, followed by a detailed sensitivity analysis. Based on these outcomes, potential strategies for the CF reduction are evaluated, after which the CF of LIBs at the pack level is assessed. Finally, the chapter discusses given limitations, outlines future research direction, and considers the wider relevance of the results for different stakeholders.

4.1. Influence of new graphite datasets on the CF of the LIB cell production

A comparative analysis of the CF and input share distribution for 1 kWh LIB cell (NMC_{622}) production under the reference and baseline scenario is shown in Fig. 5. The baseline scenario results in a CF that is approximately 1.6 times higher than in the case of the reference scenario with 93 kg CO_2eq. kWh^{-1} versus 58 kg CO_2eq. kWh^{-1}. This is primarily driven by the adoption of new environmental datasets for graphite, which show substantially higher impacts (53 kg CO_2eq. kg^{-1} BG-SG, 11 kg CO_2eq. kg^{-1} BG-NG) compared to the old database for BG graphite in Ecoinvent V 3.7.1 and before (1.9 kg CO_2eq. kg^{-1}). The CF of both BG-SG and BG-NG are slightly higher than those reported in the original studies (42.2 kg CO_2eq. kg^{-1} BG-SG, 9.6 kg CO_2eq. kg^{-1} BG-NG) [36,40]. This difference comes mainly from the use of a Chinese electricity dataset with higher CF values compared to those in the original papers. As earlier noted in Section 3.3, in this study the electricity dataset represents the specific Chinese regions where most of the BG graphite is produced, rather than the national average electricity mix. In addition, the original studies relied on the Sphera database for background processes, which may report slightly different values than the Ecoinvent database.

A detailed breakdown of the CF for the cell inputs for the baseline scenario shows that anode materials account for roughly 43% of total emissions (40 kg CO_2eq. kWh^{-1}), dominated by BG-SG (31 kg CO_2eq. kWh^{-1}) and BG-NG (7 kg CO_2eq. kWh^{-1}). Cathode materials also make a considerable contribution, and together the cathode and anode account for about 75% of the overall impacts (78 kg CO_2eq. kWh^{-1}). In contrast, cell manufacturing energy contributes less than 15% to the total, reflecting both lower energy requirements relative to earlier LCA studies [16–18,21,28,29,34,122] and the lower carbon intensity of the German electricity grid (470 g CO_2eq. kWh^{-1}). In fact, when using the Chinese electricity grid values, this share would rise to roughly 20% of total emissions, underscoring the importance of the selection of the production site.

Earlier LCA studies [16,18,21,28,29,34] identified the cell manufacturing energy as the dominant hotspot for the LIB production. However, more recent studies by von Drachenfels et al. [20] and Degen et al. [133] found that earlier estimates were overstated and demonstrated that the manufacturing energy demand decreases with an increasing energy density of the LIB cells. They reported a current cell manufacturing energy for nickel-cathode-based LIBs in the range of 20–32 kWh kWh^{-1}, resulting in a shift of the primary hotspot to the cathode materials, particularly under conditions of higher renewable shares in the grid, as reflected in the reference scenario. Building on these findings, the baseline scenario in this study, characterized by reduced cell manufacturing energy combined with the substantially higher impacts of new graphite datasets, reveals a further hotspot shift from the cathode to the anode materials, with graphite now representing the largest contributor to the CF of the LIB cell production.

Beyond climate change, the impact of new graphite datasets affects additional impact categories. Compared to the reference scenario, the

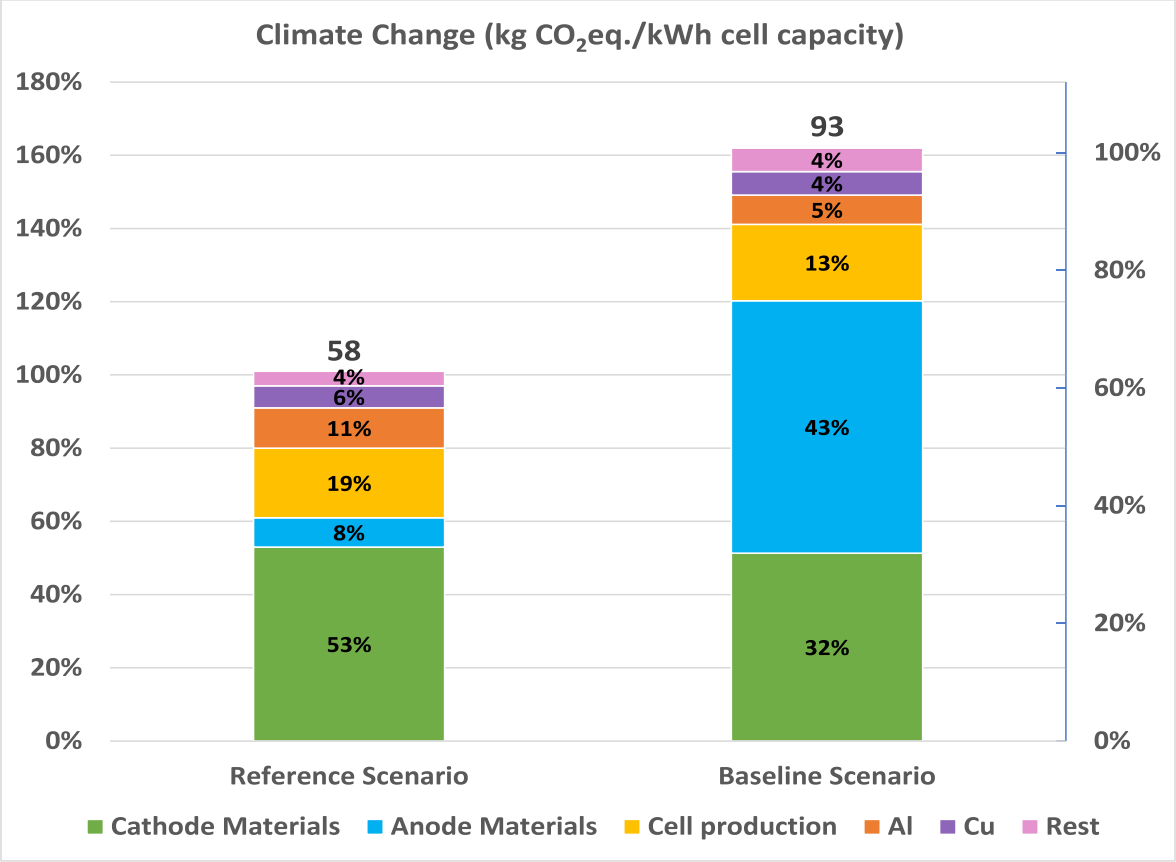

Fig. 5. Comparison of the CF and input share distribution for 1 kWh of LIB cell (NMC_{622}) production employing the old graphite dataset (reference scenario) and new graphite datasets (baseline scenario). The inputs include: cathode materials (NMC_{622} as the active material, PVDF as binder, NMP as electrode preparation solvent, and carbon black); anode materials (graphite, PVDF binder, carbon black, deionized water); aluminum (as the cathode current collector, electrode tabs, and cell housing); copper (as the anode current collector, and electrode tabs); energy inputs for the cell production (electricity and heat); and other components (electrolyte, plastics (in separator and cell housing) and waste treatment process for scrap).

baseline scenario exhibits an increase in impact magnitudes ranging from none to 2.4 times across various categories (SI: Table 7). The ozone depletion category remains unchanged between the two scenarios, while the land use category experiences the largest increase, with impacts rising 2.4-fold.

4.2. Sensitivity analysis

4.2.1. Changing the ratio of the graphite types

It is of interest to understand the dynamics between the varying proportions of the two kinds of graphite and their influence on the overall CF of LIB cell production. Particular attention is given to the quantification of the extent to which the choice of the type of graphite affects the overall CF. As discussed in Section 2.1, typically, the industry predominantly employs blends of BG-SG and BG-NG in LIB anodes to balance performance, cost, and environmental considerations [36,54,59,60,134]. For high-end applications, such as premium electric vehicles, where cost constraints are less critical and an extended cycle life and fast charging capability are more important, a higher proportion of BG-SG is typically used. In contrast, consumer electronics generally favor BG-NG-rich formulations to offer acceptable performance and lower production costs [54,135].

Graphite accounts for the largest single material input by weight in LIBs, with the baseline scenario requiring approximately 1.2 kg of graphite kWh^{-1} of cell energy. The new environmental graphite datasets clearly indicate the environmental advantage of incorporating BG-NG into LIB anodes compared with BG-SG, as the CF of BG-NG is roughly five times lower than that of BG-SG. However, it is important to note that multiple other environmental concerns have been reported in connection with NG mining in the world's largest BG-NG producing country, largely due to weak environmental regulations and limited non-compliance penalties [136]. These concerns, however, are not considered in this study, because reliable data are currently unavailable. The effects of varying proportions of BG-NG in the LIB anode on the overall CF of the LIB cell production as well as their deviation from the reference scenario are represented in Fig. 6. A LIB cell with 100% BG-NG in the anode shows the lowest CF of 68 kg CO_2eq. kWh^{-1}, which is around 27% lower than the baseline scenario, but 17% higher than the reference scenario. In contrast, a LIB cell with 100% BG-SG in the anode has the highest CF of 118 kg CO_2eq. kWh^{-1}, nearly twice that of the reference scenario and nearly 27% higher than that of the baseline scenario. For every 10% increase of the BG-NG share in the LIB anode, the CF of the LIB cell production decreases by about 4% compared with the case of 100% BG-SG.

4.2.2. Increasing process efficiencies in BG-SG production

The reported overall yield of the BG-SG production in Carrère et al. [36] is quite low (around 47%), primarily due to significantly low efficiencies of the micronizing (60%) and milling steps (80%). Although Wang et al. [48] suggested a considerably higher yield for micronizing across all BG-SG plants examined in their study, explicit numbers are not provided. Nevertheless, given the substantial influence of the low micronizing yield on the CF of BG-SG, as reported in Carrère et al. [36], this section investigates the potential impact of process improvements in the micronizing step on the CF of BG-SG and, consequently, on the LIB cell production, as illustrated in Fig. 7. For every 10% improvement of

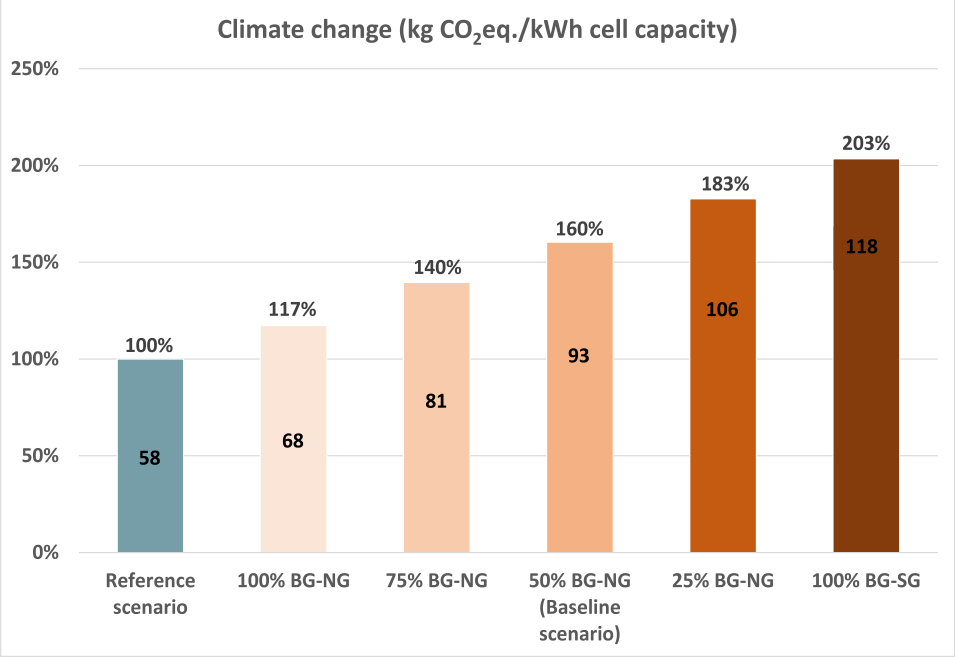

Fig. 6. Effect of varying graphite-type proportions in the anode on the CF (kg CO_2eq. kWh^{-1} cell capacity) of the LIB cell (NMC_{622}) production. The ratio indicates the proportions of BG-NG, with the remainder being BG-SG. A decreasing NG-to-SG ratio in the anode is illustrated by increasing color contrast in the figure.

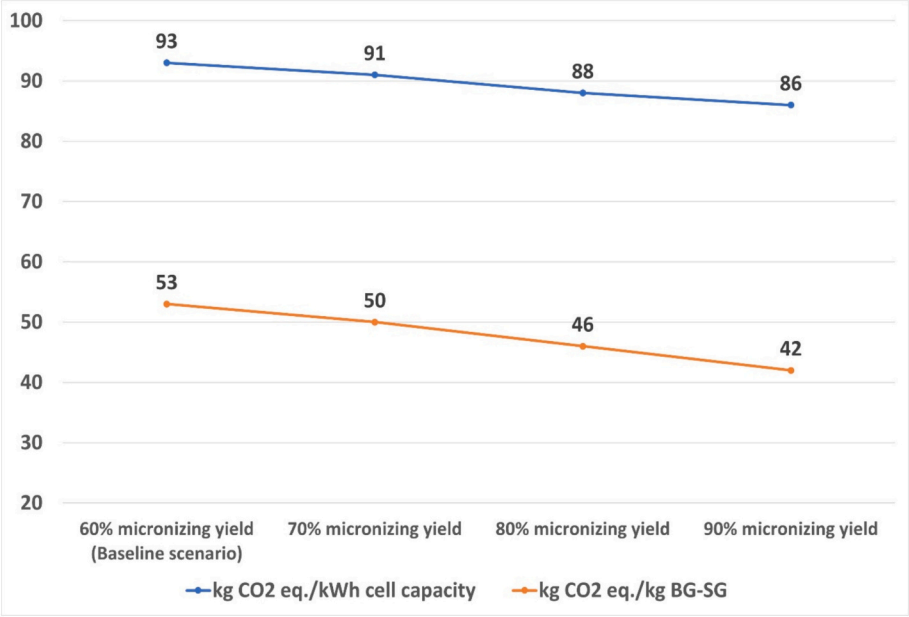

Fig. 7. Influence of yield improvement for the micronizing process on the CF of the BG-SG production and the LIB cell production.

the micronizing yield, the CF of BG-SG decreases by around 6–7%, which in turn leads to a 2–3% decrease in the CF of the LIB cell compared with the baseline scenario. When the micronizing process yield reaches 90%, the CF of LIB cell falls to 86 kg CO_2eq. kWh^{-1}, i.e., an overall decrease of around 8% relative to the baseline scenario. In contrast, improvements of other processes, such as milling and coating, exert relatively minor effects on the CF of BG-SG and are therefore not investigated further for the LIB cell production in this study. Since the electricity use is a key environmental hotspot for the BG-SG production [36], an investigation on the BG-SG production with different carbon-intensive electricity grid mixes and its effects on the CF of the LIB cells is conducted in the next section.

4.2.3. Relocating the graphite supply chains to regions powered by low-carbon electricity grids

As discussed in Section 2.3, the electricity use is the key emission hotspot for both the BG-SG and BG-NG production, while current geopolitical, trade, and policy developments are accelerating diversification and localization of graphite supply chains [90,91,137]. With the EU [90,91] and North America [138,139] advancing strategies to establish domestic graphite supply chains, and considering regional differences in electricity grid's carbon intensity, this section quantifies the environmental impacts of BG graphite produced in different regions and consequently their contribution to the overall CF of the LIB cell production.

Fig. 8 illustrates the CF of the LIB cell production (purple line) with BG graphite produced under varying electricity grid carbon intensities (green-blue line). A 10% reduction in grid CO_2eq. emissions results in an approximately 8% decrease in the CO_2eq. emissions of graphite production (combined across both graphite types). As discussed in Section 2.2, the majority of the current BG graphite production is concentrated in the northern, eastern, and southwestern regions of China, and the baseline scenario considering the BG graphite from these regions results in a CF of 93 kg CO_2eq. kWh^{-1} for the LIB cell production. In contrast, LIB cells produced with BG graphite from the northeast (historically the dominant region for both synthetic and natural graphite) exhibit the highest CF of 105 kg CO_2eq. kWh^{-1} due to the region's relatively carbon-intensive electricity grid (1.4 kg CO_2eq. kWh^{-1}). Differently, the LIB cell production using BG graphite from Europe and North America shows significantly lower CF values of around 72 and 76 kg CO_2eq. kWh^{-1}, respectively, compared to both the northeast and baseline scenario regions in China.

As highlighted earlier in this study, China's push to carbon neutrality is leading an expansion of BG graphite production in the southwest region of Country [87,88]. With the southwest region's excess renewable energy, BG graphite produced from this region will have a significantly lower CF. LIB cells with BG graphite produced in the southwest region with the current electricity grid mix will lead to a similar CF of the LIB cells as in the case of Europe and North America as production sites. Nonetheless, most of the strategic projects from CRMA dealing with the processing and extraction of BG graphite are based in countries where the CF of current electricity grid is comparatively lower than the average of Europe's electricity grid (e.g., Sweden, Norway, Finland, Greenland, and France), thus, maintaining an environmental advantage over BG graphite produced in China's southwest province. Overall, BG graphite produced within the EU, where renewables are projected to account for approximately 66% of the electricity generation by 2030 [140], is expected to maintain a lower CF compared with that produced in China (around 50% renewables) [141] and North America (about 60% renewables) [142–145]. However, a further aggressive push to increase the renewables at the European level will be beneficial for a long-term competitiveness from an environmental standpoint. Furthermore, from a broader environmental perspective, the EU's stricter mining and environmental regulations provide an additional advantage in sourcing BG graphite (NG) domestically, compared to the current leading BG-NG producing country [136].

4.2.4. *Changing the cell specific energy and comparison of the CF of LFP- and NMC-based LIB cells*

Currently, two cathode chemistries dominate the LIB market: LFP and NMC [146], each offering distinct specific energies. NMC cathodes typically deliver higher specific energy, ranging from 140 to 300 Wh kg^{-1}, compared to 90 to 200 Wh kg^{-1} for LFP [147]. Cell specific energy is a key parameter affecting the EF of LIBs [12]. A higher specific energy reduces the required amount of battery to store a given amount of energy, thereby lowering the associated EF [122]. To improve the comparability of results with other studies and investigate the influence of graphite compositions in comparison of different LIB cathode chemistries such as LFP and NMC, a LFP cell is modelled with the modelling parameters provided in Section 3.3. Fig. 9 confirms that the CF of the LIB cell production for both NMC and LFP decreases constantly with an increasing specific energy. The NMC-based LIB cell is depicted by orange lines of varying contrast, while the data for the LFP-based LIB cell is presented via blue lines of varying contrast. A higher contrast represents a relatively higher share of BG-SG than BG-NG, whereas lower contrast indicates a relatively lower share of BG-SG than BG-NG.

For the same specific energy at cell level (i.e., high-energy LFP and low-energy NMC cells) and the same graphite composition (i.e., the ratio of BG-NG and BG-SG), the NMC cell has higher CF than the LFP cell,

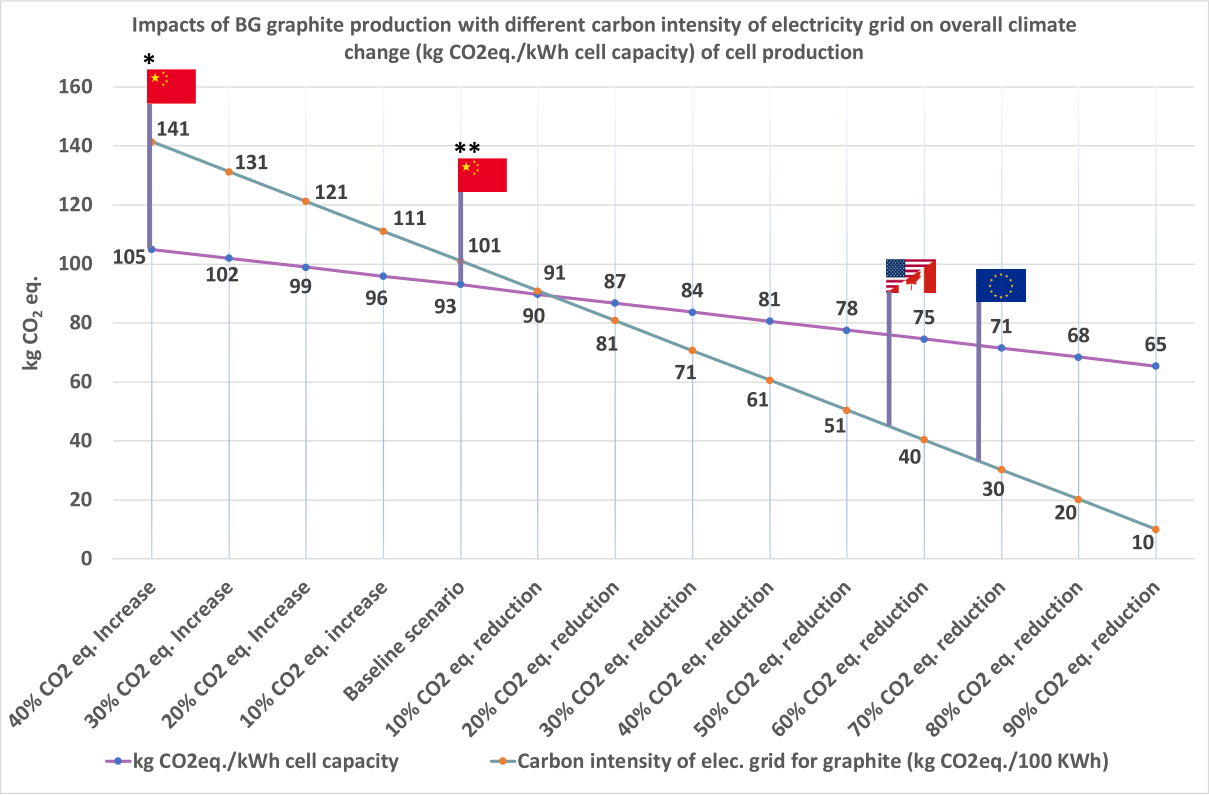

Fig. 8. The CF (kg CO_2eq. kWh^{-1} cell capacity) of the LIB production (in Germany) with BG graphite produced in different regions (China, North America (USA, Canada), and Europe).
* represents The Northeast-grid of China where ** represents the state-grid corporation of China (representing all grid mixes of China except western grid).

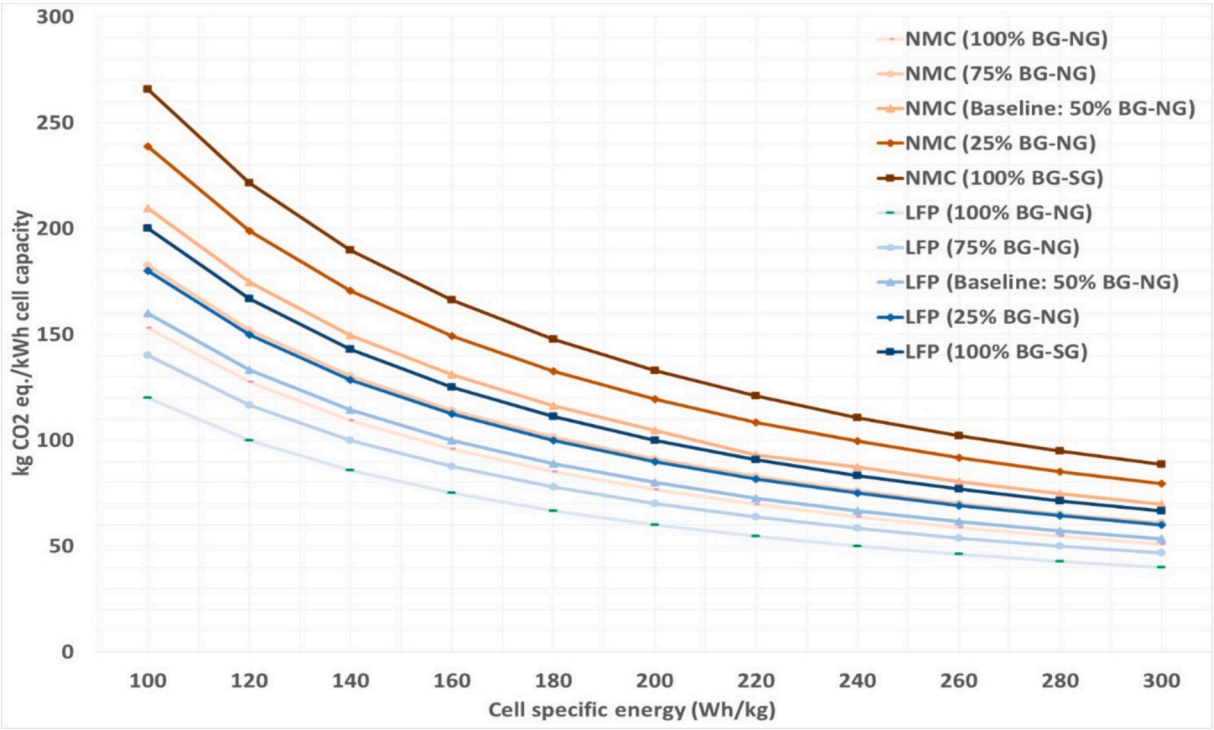

Fig. 9. Influence of the cell specific energy on the CF (kg CO_2eq. kWh^{-1} cell capacity) for the LIB cell production (for NMC-based LIBs: orange lines with varying contrast for different graphite compositions in the anode; for LFP-based LIBs: blue lines with varying contrast for different graphite compositions in the anode). (For interpretation of the references to color in this figure legend, the reader is referred to the web version of this article.)

primarily due to the higher impact of NMC compared to LFP. These results challenge earlier findings, reporting a higher CF for LFP compared to NMC for the same specific energy [122]. However, these estimates on the influence of the cell specific energy on the CF of the LIB cell production are primarily based on a simple linear scaling approach, rather than a detailed re-dimensioning of the LIB cell by adjusting the electrochemical parameters of the active materials. As a result, electrochemical limitations are not considered; for instance, achieving the same specific energy requires a higher proportion of graphite in LFP cells compared to NMC cells, due to LFP's lower cell voltage.

Moreover, Fig. 9 demonstrates the importance of the graphite composition for this comparison of the CF of LFP and NMC LIB cells. For instance, LFP with 25% BG-NG and NMC with 75% BG-NG have similar CF for the same cell specific energy. While LFP with≤50% BG-NG has a higher CF than NMC with 100% BG-NG, showcasing the importance of choosing specific graphite compositions especially for benchmarking studies. However, it is important to emphasize that the assumption of the same specific energy for LFP and NMC cells is rather hypothetical, and thus the comparison of the CF between these two cathode chemistries with different ratios of the types of graphite. Including the use-phase could alter these results, as the varying ratios of graphite types in NMC and LFP cells may impact their performance and durability. For example, cells with a high share of BG-SG have frequently a longer cycle life than cells with a lower share of BG-SG [54,57,70], which, in return, has an effect on the CF over the full cycle life of such LIB cells. Moreover, LFP cells generally possess a longer cycle life than NMC cells, which would further affect the overall CF when the use-phase is considered [34,148,149].

The CF values for LFP cells are compared with the recent studies from Sprengelmeyer et al. [127] and Voß et al. [126], who estimated a CF of 66 kg CO_2eq. kWh^{-1} and 71.2 kg CO_2eq. kWh^{-1}, respectively. Applying the same numbers for the cell specific energy (~180 Wh kg^{-1}) and the BG-NG share (75%) from Sprengelmeyer et al. [127] results in a comparable CF of 77 kg CO_2eq. kWh^{-1} (Fig. 9). The slight variation in CF is likely to come from different mass composition of cell materials and the use of a different background dataset (Sphera) by Sprengelmeyer et al. [127]. In fact, especially the CF values for both graphite types are slightly higher than those reported earlier [36,40] and used in Sprengelmeyer et al. [127], as explained in Section 4.1. Applying the same numbers for the cell specific energy (176.6 Wh kg^{-1}) and the BG-NG share (25%) as in Voß et al. [126], the calculations presented in Fig. 9 yield a significantly higher CF of 135 kg CO_2eq. kWh^{-1}. The low CF values reported by Voß et al. [126] are primarily due to the specific LCI modelling approach used by the authors for both BG-NG and BG-SG, that led to a significantly lower CF for both graphite types, as explained in Section 2.4.

4.3. *Influence of new graphite datasets on the CF at pack level*

As mentioned in Section 3.1, an expansion of the system boundary to the pack level is included to investigate the impact of our results at the pack level. Hence, additional components such as the battery management system (BMS) and the pack housing have been included in the system boundary of the cell production for a pack design (Fig. 10). The share of the BMS, pack housing, and the cells in the pack are 4.7%, 18.6%, and 76.7%, respectively [34]. The specific energy at the pack level is 172 Wh kg^{-1}. The LCI for the BMS and pack housing are extracted from Peters et al. [130], who used the data reported by Ellingsen et al. [16] for the BMS, and the data reported by Majeau-Bettez et al. [29] for the pack housing. The energy consumption for the pack assembly is considered zero in this study, following the rational of Erakca et al. [19], where the authors stated that either the impact of the energy demand for the pack assembly was found to be minimal or that a manual process has been considered for the pack assembly in the existing literature (Ellingsen et al. [16], Dai et al. [17]).

Similar to the impacts at cell level, the baseline scenario results in a CF about 1.5 times higher than the reference scenario, i.e., 105 kg CO_2eq. kWh^{-1} compared to 70 kg CO_2eq. kWh^{-1}, as shown in Fig. 11. As expected, in the baseline scenario, around 90% of the overall CF come from the cell, and the BMS and pack housing contributing around 7%

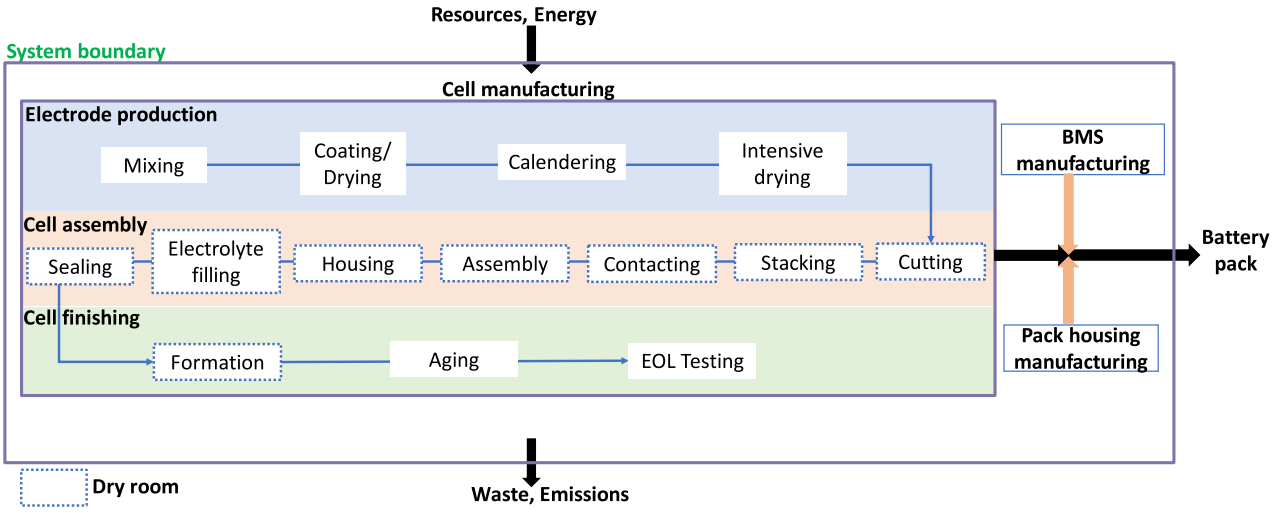

Fig. 10. System boundary for the battery pack. Schematic representation inspired by Erakca et al. [19].

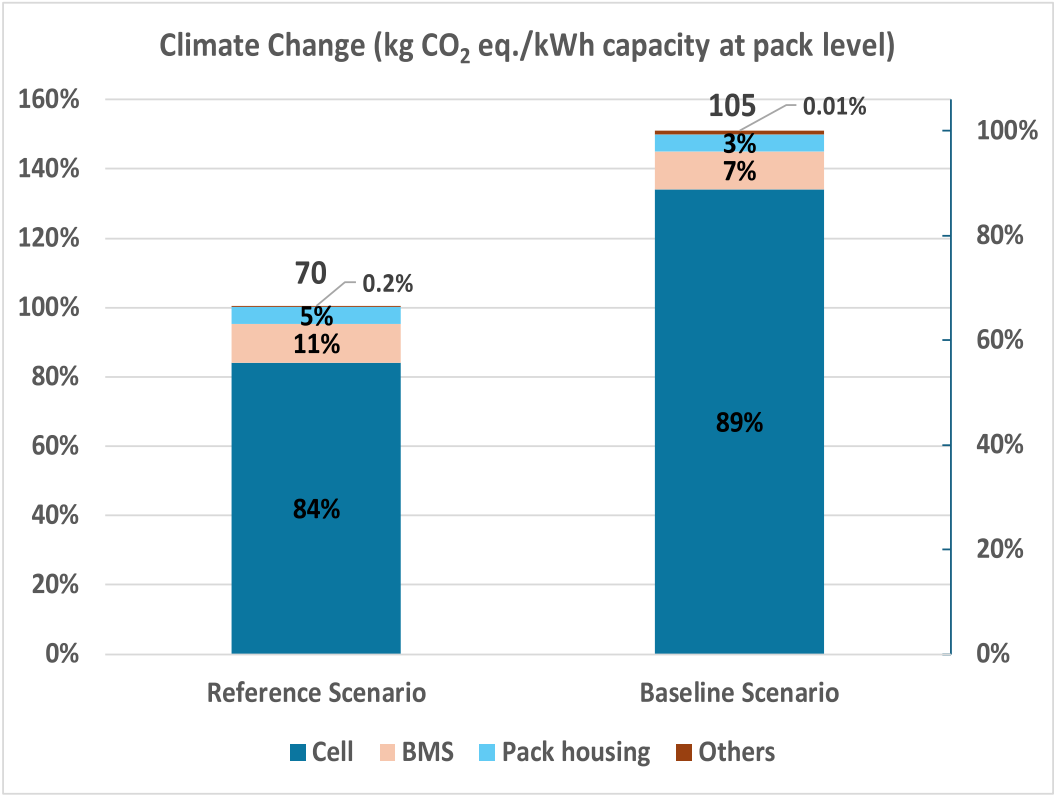

Fig. 11. Comparison of the CF for 1 kWh of battery pack (the reference scenario represents the NMC_{622} cell production with the old graphite dataset [110] and the baseline scenario represents the cell production with the new graphite datasets [36,40]).

and 3%, respectively. In the reference scenario, the share of the cell-related impacts is slightly lower, at about 84%. This reduction is primarily due to the older BG graphite dataset in the reference scenario, which has lower impacts compared to the new datasets used in the baseline scenario.

4.4. Limitations and future work

While this study provides key findings on the critical role of BG graphite and its compositions (BG-NG and BG-SG) in the anode on the CF of the LIB cell production and valuable insights on their influencing factors, some limitations must be acknowledged before interpreting the results.

Regarding the data, the CF values of the LIB cell production are derived from the data based on primary industrial sources for both cell production and BG graphite (BG-NG and BG-SG). Since the LCI data for both graphite types are incorporated in major environmental databases, the results can be seen as representative and robust. However, they may not capture the company specific variations in process efficiencies, and the energy and material consumption for graphite production. For example, emerging technologies such as the closed furnace technology from e.g. Vianode and continuous graphitization technology will

decrease the CF for SG significantly and widespread adoption of such processes in future may alter the CF hotspots landscape of the LIB production. Similarly, the data on cell manufacturing energy and bill of materials for the LIB cells are based on a single German factory and may not account for differences arising from local environmental conditions, production throughput, alternative manufacturing processes, and different cell formats. Thus, considering the rapid pace of innovation in battery field, the datasets need to be updated regularly to keep pace with ongoing developments and to prevent outdates conclusions and misleading recommendations.

From the methodological and modelling perspective, like in any LCA studies, the results are sensitive to the choice of allocation (physical allocation, economic allocation, or system expansion) and LCIA methods. In this study, economic allocation and no-allocation are considered for the co-products in the BG-SG and BG-NG production, respectively, in line with the original sources. Since the choice of allocation depends on several factors and is subject to change, depending on the co-products' relevance within the system or in the market, applying different allocation methods in the future could either increase or decrease the CF of BG graphite, and subsequently of that of the LIB cell production as a whole.

Another limitation related to the system boundary is that transportation activities are excluded because of their relatively minor contribution to the overall CF of the LIB cell production. Furthermore, the present study considered only cradle-to-gate impacts and excluded the use-phase and EoL. However, the ratio of BG-NG to BG-SG in LIB anodes has a decisive influence on the use-phase. As shown in Table 1, LIBs with a higher share of BG-SG in the anode frequently achieve longer cycle life, and improved safety compared to BG-NG, which can ultimately decrease the CF over the battery lifetime. Hence the decision for a certain ratio of BG-NG to BG-SG depends, besides the CF, much more on the desired performance and intended application. As this study identifies graphite as a key hotspot in the CF of LIB cell production, future research should consider the potential benefits of large-scale graphite recycling within broader LIB cell recycling strategies. Overall, the future work should address the full life cycle of BG graphite in LIBs by incorporating data on the cycle life and performance for different BG-NG to BG-SG ratios, together with their recycling, in order to provide more robust insights into the optimal balance between BG-NG and BG-SG in LIB anodes.

4.5. Implications of the results

The findings of this study carry important implications for multiple stakeholder groups. For LCA practitioners, the results highlight that, with the new environmental graphite datasets, graphite emerges as a key hotspot in the CF of the LIB cell production. Moreover, the CF is highly sensitive to the choice and proportion of the graphite types used in the anode, meaning that variations of SG-to-NG ratio can alter the CF of the LIB significantly and influence the benchmarking outcomes when comparing LIBs with SIBs, where hard carbon replaces graphite in the anode. Proper benchmarking of recycled graphite, either against the actual CF of the graphite mix used in LIB cells or the CF of the graphite mix it replaces, will be essential to accurately measure the environmentally friendliness of graphite recycling.

For battery researchers and manufacturers, the findings indicate that prioritizing BG-NG over BG-SG can lower the CF in LIB cell production, provided that comparable performance during the use-phase is ensured. Nevertheless, the current limitation is that NG-based anodes often exhibit shorter cycle life and lower thermal stability than BG-SG, which may offset the initial climate benefits over the full battery lifetime. Therefore, further research is required to enhance the electrochemical performance and durability of BG-NG in order to bridge this gap. Efforts to increase process efficiency in graphite production- particularly for BG-SG, where yields remain at ~50%- will also be essential, alongside the electrification of production processes as a key strategy for emission reductions. In parallel, exploring anode-free LIB, alternative anode materials such as silicon or bio-based graphite and incorporating recycled graphite into LIB anodes represent promising pathways for reducing CF. For recyclers, the results underscore the importance of giving graphite recycling a role comparable to that of high-value cathode materials such as nickel and cobalt.

Finally, the results of this study carry important implications for policy-making. Accelerating the transition to renewable energy is essential to lowering the CF of both graphite and LIB production. Equally, investing in domestic graphite projects is essential for strengthening local supply chains and maintaining environmental competitiveness. Furthermore, setting explicit targets for graphite recovery from end-of-life batteries and minimum recycled graphite requirements in new batteries into the EU's battery regulation would significantly strengthen the resilience and sustainability of the European graphite sector.

5. Conclusion

This study addresses the existing knowledge gap on the selection and proportions of BG-NG and BG-SG for anode in the CF of LIB cell production. It reviews their current production processes, supply chains, and evaluates existing LCA studies for data quality, representativeness, and inclusion in environmental databases. The review reveals that most studies relied on outdated and non-transparent secondary data, included incomplete process chains, and are not representative of current industrial practices, leading to a misrepresentation of BG graphite impacts in the CF of LIB cell. Recent LCA studies by Carrère et al. [36] and Engels et al. [40], based on primary industrial data for both graphite types, show significantly higher impacts, highlighting the need to reassess the CF of LIB cell production using new BG-NG and BG-SG datasets.

The results indicate that the CF of LIB cell production for a baseline scenario (equal share of BG-NG and BG-SG in the anode) increases sharply from previously reported number in the recent LCA study. Furthermore, the results present a new finding on the CF hotspot, shifting from CAMs or cell manufacturing energy to BG graphite. Building up on this new finding, the study further investigates the critical role of BG graphite composition, and shows that the choice of the type of graphite and its mixture in varying proportions in the LIB anode has a significant influence on the CF of the LIB cell production, with a relatively higher share of BG-NG compared to BG-SG leading to a substantial reduction in the overall CF. As the electricity use is a key hotspot for the production of both graphite types, the findings emphasize that sourcing BG graphite from regions with a high share of renewable electricity provides a greater potential for CF reduction. In addition, the study challenges previous LCA results, showing that for the same cell specific energy the production of LFP-based LIBs has lower CF than in the case of NMC-based LIBs, primarily due to the use of lower-impact CAMs in the LFP-based LIBs compared to NMC-based LIBs.

Since the results are derived from primary industrial data on both BG graphite and cell manufacturing, these can be seen as robust and representative, though certain limitations from the data, methodology and modelling perspectives should be kept in mind before interpreting the results in future. For example, the findings on CF of LIB cell with varying BG graphite types share reflects only the production stage; including the use-phase and EoL data in the future may alter these findings. Moreover, emerging technologies such as continuous graphitization for continuous BG-SG production and close furnace technology hold the potential for improving production efficiency and could substantially reduce the CF in the future. However, the findings are highly relevant for multiple stakeholder groups: battery manufacturers should, where feasible, prioritize BG-NG, enhance BG-SG efficiency, and explore alternative materials; LCA practitioners should carefully account for graphite ratios in anodes, as these influence benchmarking; and policymakers should promote renewable energy, support domestic graphite production, and implement recovery and recycled content targets to

strengthen the sustainability and resilience of the European graphite and LIB sector. Finally, given the critical role of BG graphite in the LIB cell, there is a must that both existing and emerging recycling technologies achieve high efficiencies in recovering anode materials in battery grade quality.

CRediT authorship contribution statement

Pushpendra: Writing – review & editing, Writing – original draft, Visualization, Validation, Methodology, Investigation, Data curation, Conceptualization. **Elias Vollert:** Writing – review & editing. **Dominic Bresser:** Writing – review & editing. **Marcel Weil:** Writing – review & editing, Supervision, Funding acquisition, Formal analysis, Conceptualization.

Declaration of Generative AI and AI-assisted technologies in the writing process

During the preparation of this work Pushpendra used Paperpal, Perplexity (perplexity AI), and ChatGPT 5.0 in order to revise sentence structure, and grammar checking. After using these tools, the authors reviewed and edited the content as needed and take full responsibility for the content of the publication.

Declaration of competing interest

The authors declare that they have no known competing financial interests or personal relationships that could have appeared to influence the work reported in this paper.

Acknowledgements

The authors acknowledge the financial support from the German Research Foundation (DFG) under Project ID 390874152 (POLiS Cluster of Excellence, EXC 2154) and the European Union's Horizon 2020 - Research and Innovation Framework Programme under Grant Agreements Ns 101137745 (RENOVATE). We are especially thankful to Uldrico Ulissi from Contemporary Amperex Technology Co. Limited (CATL) and Teo Lombardo from the International Energy Agency (IEA) for providing their valuable inputs on synthetic graphite producers. We also sincerely thank Margo Stokebrand from Institut für Technikfolgenabschätzung und Systemanalyse - Karlsruhe Institute of Technology (ITAS-KIT), for her assistance in preparing the graphical abstract, figure formatting and visualization, and providing key support on global distribution on graphite producers.

Open access funding enabled and organized by project DEAL.

Appendix A. Supplementary data

Supplementary data to this article can be found online at https://doi.org/10.1016/j.est.2026.121887.

Data availability

Data will be made available on request.

References

[1] European Commission, 2040 climate target. European Commission, 2024. Available from: https://climate.ec.europa.eu/eu-action/climate-strategies-targets/2040-climate-target_en (Internet, cited 2025 May 14).
[2] Dennis Seibert, P. Kasten, J. Graichen, N. Wissner, EU 2040 Climate target: contributions of the transport sector, 2024. Available from: https://www.oeko.de/fileadmin/oekodoc/EU2040ClimateTarget_potential-contributions-of-transport_final.pdf (Internet).
[3] Regulation (EU) 2023/851 of the European Parliament and of the Council of 19 April 2023 amending Regulation (EU) 2019/631 as regards strengthening the CO2 emission performance standards for new passenger cars and new light commercial vehicles in line with the Union's increased climate ambition (text with EEA relevance), 2023. Available from: https://eur-lex.europa.eu/legal-content/EN/TXT/PDF/?uri=CELEX:32023R0851 (Internet, cited 2025 May 14).
[4] M. Weil, J. Peters, M. Baumann, Chapter 5-stationary battery systems: future challenges regarding resources, recycling, and sustainability, in: A. Bleicher, A. Pehlken (Eds.), The Material Basis of Energy Transitions, Academic Press, 2020, pp. 71–89. Available from: https://www.sciencedirect.com/science/article/pii/B9780128195345000052 (cited 2025 Sep 8, Internet).
[5] E. Laabs, T. Kind-Rieper, K. Engel, S. Hall, J.P.T. Miranda, T. Vahle, et al., Bringing Batteries Production to Europe: In a Green and Responsible Way, WWF Germany, 2024. Available from: https://www.wwf.de/fileadmin/fm-wwf/Publikationen-PDF/Wald/wwf-study-green-responsible-batterie-production-eu.pdf (Internet).
[6] Regulation (EU) 2023/1542 of the European Parliament and of the Council of 12 July 2023 concerning batteries and waste batteries, amending Directive 2008/98/EC and Regulation (EU) 2019/1020 and repealing Directive 2006/66/EC (Text with EEA relevance), OJ L (Jul 12, 2023). Available from: http://data.europa.eu/eli/reg/2023/1542/oj/eng (Internet).
[7] T. Hettesheimer, C. Neef, I. Rosellón Inclán, S. Link, T. Schmaltz, F. Schuckert, et al., Lithium-ion Battery Roadmap-Industrialization Perspectives Toward 2030, 2023, https://doi.org/10.24406/publica-2153 (cited 2025 Sep 28).
[8] J.B. Dunn, L. Gaines, J.C. Kelly, C. James, K.G. Gallagher, The significance of Li-ion batteries in electric vehicle life-cycle energy and emissions and recycling's role in its reduction, Energy Environ. Sci. 8 (1) (Dec 18 2014) 158–168.
[9] A. Nordelöf, M. Messagie, A.M. Tillman, M. Ljunggren Söderman, J. Van Mierlo, Environmental impacts of hybrid, plug-in hybrid, and battery electric vehicles—what can we learn from life cycle assessment? Int. J. Life Cycle Assess. 19 (11) (Nov 1 2014) 1866–1890.
[10] C. Bauer, J. Hofer, H.J. Althaus, A. Del Duce, A. Simons, The environmental performance of current and future passenger vehicles: life cycle assessment based on a novel scenario analysis framework, Appl. Energy (157) (Nov 1 2015) 871–883.
[11] M. Weil, J. Peters, M. Baumann, H. Dura, B. Zimmermann, Elektrochemische Energiespeicher für mobile Anwendungen im Fokus der Systemanalyse, TATuP J. Technol. Assess. Theory Pract. 24 (3) (Nov 1 2015) 20–29.
[12] J.F. Peters, M. Baumann, B. Zimmermann, J. Braun, M. Weil, The environmental impact of Li-ion batteries and the role of key parameters – a review, Renew. Sust. Energ. Rev. 67 (Jan 1 2017) 491–506.
[13] Q. Chen, X. Lai, J. Chen, Y. Huang, Y. Guo, Y. Wang, et al., A critical comparison of LCA calculation models for the power lithium-ion battery in electric vehicles during use-phase, Energy 296 (Jun 1 2024) 131175.
[14] Q. Chen, X. Lai, Y. Zhang, J. Chen, Z. Zhu, Y. Huang, et al., Environmental impacts and supply risks for LiFePO4 - LiCoxNiyMn1-x-yO2 hybrid battery pack in China, Process. Saf. Environ. Prot. 198 (Jun 1 2025) 107115.
[15] Nigel, Cell to pack mass ratio, Available from:, Battery Design, 2022. https://www.batterydesign.net/cell-to-pack-mass-ratio/.
[16] L.A.W. Ellingsen, G. Majeau-Bettez, B. Singh, A.K. Srivastava, L.O. Valøen, A. H. Strømman, Life cycle assessment of a lithium-ion battery vehicle pack, J. Ind. Ecol. 18 (1) (2014) 113–124.
[17] Q. Dai, J.C. Kelly, L. Gaines, M. Wang, Life cycle analysis of lithium-ion batteries for automotive applications, Batteries 5 (2) (Jun 2019) 48.
[18] M. Chordia, A. Nordelöf, L.A.W. Ellingsen, Environmental life cycle implications of upscaling lithium-ion battery production, Int. J. Life Cycle Assess. (26) (Oct 1 2021) 2024–2039.
[19] M. Erakca, S. Pinto Bautista, S. Moghaddas, M. Baumann, W. Bauer, L. Leuthner, et al., Closing gaps in LCA of lithium-ion batteries: LCA of lab-scale cell production with new primary data, J. Clean. Prod. 384 (Jan 15 2023) 135510.
[20] N. von Drachenfels, J. Husmann, U. Khalid, F. Cerdas, C. Herrmann, Life cycle assessment of the battery cell production: using a modular material and energy flow model to assess product and process innovations, Energ. Technol. 11 (5) (2023) 2200673.
[21] H.C. Kim, T.J. Wallington, R. Arsenault, C. Bae, S. Ahn, J. Lee, Cradle-to-gate emissions from a commercial electric vehicle Li-ion battery: a comparative analysis, Environ. Sci. Technol. 50 (14) (Jul 19 2016) 7715–7722.
[22] S. Jiang, L. Zhang, F. Li, H. Hua, X. Liu, Z. Yuan, et al., Environmental impacts of lithium production showing the importance of primary data of upstream process in life-cycle assessment, J. Environ. Manag. 262 (May 15 2020) 110253.
[23] S. Ahmed, P.A. Nelson, K.G. Gallagher, N. Susarla, D.W. Dees, Cost and energy demand of producing nickel manganese cobalt cathode material for lithium ion batteries, J. Power Sources (342) (Feb 28 2017) 733–740.
[24] S.H. Farjana, N. Huda, M.A.P. Mahmud, Life cycle assessment of cobalt extraction process, J. Sustain. Min. 18 (3) (Aug 1 2019) 150–161.
[25] M. Mistry, J. Gediga, S. Boonzaier, Life cycle assessment of nickel products, Int. J. Life Cycle Assess. 21 (11) (Nov 1 2016) 1559–1572.
[26] P.T. Benavides, Q. Dai, J.L. Sullivan, J.C. Kelly, J.B. Dunn, Material and Energy Flows Associated With Select Metals in GREET 2. Molybdenum, Platinum, Zinc, Nickel, Silicon, Argonne National Lab. (ANL), Argonne, IL (United States), Sep 2015. Report No.: ANL/ESD-15/11. Available from: https://www.osti.gov/biblio/1224976 (cited 2025 May 16, Internet).
[27] R. Yin, S. Hu, Y. Yang, Life cycle inventories of the commonly used materials for lithium-ion batteries in China, J. Clean. Prod. (227) (Aug 1 2019) 960–971.
[28] M. Zackrisson, L. Avellán, J. Orlenius, Life cycle assessment of lithium-ion batteries for plug-in hybrid electric vehicles – critical issues, J. Clean. Prod. 18 (15) (Nov 1 2010) 1519–1529.
[29] G. Majeau-Bettez, T.R. Hawkins, A.H. Strømman, Life cycle environmental assessment of lithium-ion and nickel metal hydride batteries for plug-in hybrid

and battery electric vehicles, Environ. Sci. Technol. 45 (10) (May 15 2011) 4548–4554.
[30] M. Chordia, S. Wickerts, A. Nordelöf, R. Arvidsson, Life cycle environmental impacts of current and future battery-grade lithium supply from brine and spodumene, Resour. Conserv. Recycl. (187) (Dec 1 2022) 106634.
[31] V. Schenker, C. Oberschelp, S. Pfister, Regionalized life cycle assessment of present and future lithium production for Li-ion batteries, Resour. Conserv. Recycl. (187) (Dec 1 2022) 106611.
[32] L. Peiseler, V. Schenker, K. Schatzmann, S. Pfister, V. Wood, T. Schmidt, Carbon footprint distributions of lithium-ion batteries and their materials, Nat. Commun. 15 (1) (Nov 27 2024) 10301.
[33] V. Schenker, S. Pfister, Current and future impacts of lithium carbonate from brines: a global regionalized life cycle assessment model, Environ. Sci. Technol. 59 (13) (Apr 8 2025) 6543–6555.
[34] M. Mohr, J.F. Peters, M. Baumann, M. Weil, Toward a cell-chemistry specific life cycle assessment of lithium-ion battery recycling processes, J. Ind. Ecol. 24 (6) (2020) 1310–1322.
[35] P. Engels, N. Kononova, U. Khalid, F. Cerdas, C. Herrmann, Methodology for a combined uncertainty analysis and data quality rating of existing graphite datasets in context of battery LCAs, Procedia CIRP (105) (Jan 1 2022) 577–582.
[36] T. Carrère, U. Khalid, M. Baumann, M. Bouzidi, B. Allard, Carbon footprint assessment of manufacturing of synthetic graphite battery anode material for electric mobility applications, J. Energy Storage (94) (Jul 30 2024) 112356.
[37] S. Wang, K.V. Kravchyk, F. Krumeich, M.V. Kovalenko, Kish graphite flakes as a cathode material for an aluminum chloride–graphite battery, ACS Appl. Mater. Interfaces 9 (34) (Aug 30 2017) 28478–28485.
[38] Z. Wang, B. Xing, H. Zeng, G. Huang, X. Liu, H. Guo, et al., Space-confined carbonization strategy for synthesis of carbon nanosheets from glucose and coal tar pitch for high-performance lithium-ion batteries, Appl. Surf. Sci. 547 (May 1 2021) 149228.
[39] Z. Wang, D. Zhang, X. Bao, R. Hong, Y. Xu, J. Xu, et al., Space-confined intercalation expansion strategy for simple and rapid synthesis of kish-based expanded graphite for aluminum ion batteries, Carbon 223 (Apr 10 2024) 119016.
[40] P. Engels, F. Cerdas, T. Dettmer, C. Frey, J. Hentschel, C. Herrmann, et al., Life cycle assessment of natural graphite production for lithium-ion battery anodes based on industrial primary data, J. Clean. Prod. 336 (Feb 15 2022) 130474.
[41] J. Park, S.J. Cho, S. Shin, R. Kim, D. Shin, Y. Shin, Overview of graphite supply chain and its challenges, Geosci. J. 29 (3) (Jun 1 2025) 329–341.
[42] D. Surovtseva, E. Crossin, R. Pell, L. Stamford, Toward a life cycle inventory for graphite production, J. Ind. Ecol. 26 (3) (2022) 964–979.
[43] Ecoinvent. graphite production, battery grade - China - graphite, battery grade, ecoQuery, 2022. Available from: https://ecoquery.ecoinvent.org/3.9.1/cutoff/dataset/3576/documentation (cited 2025 Sep 10, Internet).
[44] D.A. Notter, M. Gauch, R. Widmer, P. Wäger, A. Stamp, R. Zah, et al., Contribution of Li-ion batteries to the environmental impact of electric vehicles, Environ. Sci. Technol. 44 (17) (Sep 1 2010) 6550–6556.
[45] E. Kallitsis, A. Korre, G. Kelsall, M. Kupfersberger, Z. Nie, Environmental life cycle assessment of the production in China of lithium-ion batteries with nickel-cobalt-manganese cathodes utilising novel electrode chemistries, J. Clean. Prod. (254) (May 1 2020) 120067.
[46] Z. Shi, Y. Jin, T. Han, H. Yang, R. Gond, Y. Subasi, et al., Bio-based anode material production for lithium–ion batteries through catalytic graphitization of biochar: the deployment of hybrid catalysts, Sci. Rep. 14 (1) (Feb 17 2024) 3966.
[47] A. Cherakkara, S. Zafar, I. Izwan Misnon, C.C. Yang, R. Jose, Graphite from biomass: a review on synthetic feasibility, J. Ind. Eng. Chem. (145) (May 25 2025) 75–98.
[48] F. Wang, S. Zhang, M. Liu, Y. Xiong, D. De Castro Gomez, X. He, et al., Carbon footprint and decarbonization potential of battery-grade synthetic graphite, ACS Sustain. Chem. Eng. 13 (22) (Jun 9 2025) 8298–8306.
[49] K.J. Kim, V.H. Pham, Y. Gao, N.T. Huynh, Y.Y. Lee, C. Wang, et al., Synthesizing highly crystalline graphite powder from bulk polyethylene waste for lithium-ion battery anodes, ACS Sustain. Resour. Manag. 2 (1) (Jan 23 2025) 146–156.
[50] E.E. Oseland, T.S. Rajan, M. Lain, D. Proprentner, H. Dutton, A. Bostwick, et al., Graphite development from a manufacturers perspective: processing, formation, and benchmarking, PRX Energy. 4 (4) (Nov 7 2025) 043006.
[51] R. Songthan, T. Sangsanit, K. Santiyuk, K. Homlamai, W. Tejangkura, M. Sawangphruk, Revisiting the effect of natural and artificial graphite on the performance of Ni-rich Li-ion batteries at coin and cylindrical cells, J. Electrochem. Soc. 171 (5) (May 2024) 050524.
[52] D.C. Hebestreit, Experts hearing in the framework of the opinion CCMI/211 Critical Raw Materials Act, Available from: https://www.eesc.europa.eu/sites/default/files/files/presentation_by_corina_hebestreit_-_ecga_on_critical_raw_materials_act.pdf, 2023 May 15.
[53] J. Peng, S. Maslek, N. Sharma, Spent graphite from lithium-ion batteries: re-use and the impact of ball milling for re-use, RSC Sustain. 2 (5) (2024) 1418–1430.
[54] J. Asenbauer, T. Eisenmann, M. Kuenzel, A. Kazzazi, Z. Chen, D. Bresser, The success story of graphite as a lithium-ion anode material – fundamentals, remaining challenges, and recent developments including silicon (oxide) composites, Sustain. Energy Fuels 4 (11) (Oct 27 2020) 5387–5416.
[55] R.K. Lyer, J.C. Kelly, Updated Production Inventory for Lithium-ion Battery Anodes for the GREET® Model, and Review of Advanced Battery Chemistries, Argonne National Lab. (ANL), Argonne, IL (United States), Oct 2022, https://doi.org/10.2172/1891640 (Report No.: ANL-22/74, cited 2025 May 16, Internet).
[56] K. Bhuwalka, H. Ramachandran, S. Narasimhan, A. Yao, J. Frohmann, L. Peiseler, et al., Securing the Supply of Graphite for Batteries, Cornell University, Apr 2025, https://doi.org/10.48550/arXiv.2503.21521 (Report No.: Papers 2503:21521, Internet).
[57] Robin R. Jacob, Viability and eco-consequences of synthetic and natural graphite for lithium-ion battery anodes in the USA, IEEE Eng. Manag. Rev. 52 (3) (Jun 2024) 131–147.
[58] S. Chen, C. Liu, R. Feng, Z. Chen, Y. Lu, L. Chen, et al., Natural graphite anode for advanced lithium-ion batteries: challenges, progress, and perspectives, Chem. Eng. J. 503 (Jan 1 2025) 158116.
[59] K. Adham, S. Francey, A comparison of production routes for natural versus synthetic graphites destined for battery material, in: Proceedings of the 62nd Conference of Metallurgists, COM 2023, Springer Nature Switzerland, Cham, 2023, pp. 397–403.
[60] M. Mundszinger, S. Farsi, M. Rapp, U. Golla-Schindler, U. Kaiser, M. Wachtler, Morphology and texture of spheroidized natural and synthetic graphites, Carbon (111) (Jan 1 2017) 764–773.
[61] Z. Liu, Y. Shi, Q. Yang, H. Shen, Q. Fan, H. Nie, Effects of crystal structure and electronic properties on lithium storage performance of artificial graphite, RSC Adv. 13 (43) (Oct 11 2023) 29923–29930.
[62] G. Wang, A. Mijailovic, J. Yang, J. Xiong, S.E. Beasley, K. Mathew, et al., Particle size effect of graphite anodes on performance of fast charging Li-ion batteries, J. Mater. Chem. A 11 (40) (Oct 17 2023) 21793–21805.
[63] Y.J. Choi, Y.S. Lee, J.H. Kim, J.S. Im, Optimization of pore characteristics of graphite-based anode for Li-ion batteries by control of the particle size distribution, Materials 16 (21) (Jan 2023) 6896.
[64] S. Natarajan, T. Mae, H.Y. Teah, H. Sakurai, S. Noda, Environmentally friendly regeneration of graphite from spent lithium-ion batteries for sustainable anode material reuse, J. Mater. Chem. A 13 (7) (Feb 12 2025) 4984–4993.
[65] P.P. Magampa, N. Manyala, W.W. Focke, Properties of graphite composites based on natural and synthetic graphite powders and a phenolic novolac binder, J. Nucl. Mater. 436 (1) (May 1 2013) 76–83.
[66] X. Rui, Y. Geng, M. Zhuang, S. Xiao, X. Sun, Emergy-based environmental accounting of graphite anode material production, J. Clean. Prod. (339) (Mar 10 2022) 130705.
[67] H.J. Kwon, S.W. Woo, Y.J. Lee, J.Y. Kim, S.M. Lee, Achieving high-performance spherical natural graphite anode through a modified carbon coating for lithium-ion batteries, Energies 14 (7) (Jan 2021) 1946.
[68] G. Güven, U. Ulusoy, F. Burat, B. Mojtahedi, G. Bayar, Time-dependent tap density modeling of graphite milled by vibrating disc mill, Minerals 15 (4) (Apr 2025) 403.
[69] Y. Kim, E.H. Jeong, B.S. Kim, J.D. Park, Comparative study on the rheological properties of natural and synthetic graphite-based anode slurries for lithium-ion batteries, Kor. Aust. Rheol. J. 36 (1) (Feb 1 2024) 25–32.
[70] S.L. Glazier, J. Li, A.J. Louli, J.P. Allen, J.R. Dahn, An analysis of artificial and natural graphite in lithium ion pouch cells using ultra-high precision coulometry, isothermal microcalorimetry, gas evolution, long term cycling and pressure measurements, J. Electrochem. Soc. 164 (14) (Nov 16 2017) A3545.
[71] A. Eldesoky, M. Bauer, S. Azam, E. Zsoldos, W. Song, R. Weber, et al., Impact of graphite materials on the lifetime of NMC811/graphite pouch cells: Part I. Material properties, ARC safety tests, gas generation, and room temperature cycling, J. Electrochem. Soc. 168 (11) (Nov 2021) 110543.
[72] A.D. Jara, A. Betemariam, G. Woldetinsae, J.Y. Kim, Purification, application and current market trend of natural graphite: a review, Int. J. Min. Sci. Technol. 29 (5) (Sep 1 2019) 671–689.
[73] J. Zhang, C. Liang, J.B. Dunn, Graphite flows in the U.S.: insights into a key ingredient of energy transition, Environ. Sci. Technol. 57 (8) (Feb 15 2023) 3402–3414.
[74] SCREEN Factsheets Updates Based on 2020 Factsheets: Natural Graphite, 2023, p. 36. Available from: https://scrreen.eu/wp-content/uploads/2023/12/SCRREEN2_factsheets_GRAPHITE_V1.pdf (Internet).
[75] M. Mancini, J. Martin, I. Ruggeri, N. Drewett, P. Axmann, M. Wohlfahrt-Mehrens, Enabling fast-charging lithium-ion battery anodes: influence of spheroidization on natural graphite, Batteries Supercaps 5 (7) (2022) e202200109.
[76] B. Biber, S. Sander, J. Martin, M. Wohlfahrt-Mehrens, M. Mancini, Improved production process with new spheroidization machine with high efficiency and low energy consumption for rounding natural graphite for Li-ion battery applications, Carbon (201) (Jan 5 2023) 847–855.
[77] M. Yoshio, H. Wang, K. Fukuda, Spherical carbon-coated natural graphite as a lithium-ion battery-anode material, Angew. Chem. 115 (35) (2003) 4335–4338.
[78] O. Mukhan, J.S. Yun, H. Munakata, K. Kanamura, S.S. Kim, Quantification of the carbon-coating effect on the interfacial behavior of graphite single particles, ACS Omega 9 (3) (Jan 23 2024) 4004–4012.
[79] M. Golden, Confronting China's grip on graphite for batteries, Available from:, Stanford Energy, 2025. https://energy.stanford.edu/news/confronting-chinas-grip-graphite-batteries.
[80] Benchmark Minerals Intelligence Limited. Benchmark Source, Chinese flake graphite miners feel the pressure as prices drop further in August, Available from: https://source.benchmarkminerals.com/article/chinese-flake-graphite-miners-feel-the-pressure-as-prices-drop-further-in-august, 2024 (cited 2025 Aug 16).
[81] A. Ritoe, I. Patrahau, M. Rademaker, Graphite | supply chain challenges & recommendations for a critical mineral, Available from:, The Hague Centre for Strategic Studies, Mar 2022. https://hcss.nl/wp-content/uploads/2022/03/Graphite-Challenges-and-Recommendations-HCSS-2022.pdf.
[82] Survey USG, Mineral commodity summaries 2022. Mineral commodity summaries, Available from:, U.S. Geological Survey, 2022. https://pubs.usgs.gov/publication/mcs2022.

[83] Survey USG, Mineral commodity summaries 2025. Mineral commodity summaries, Available from:, U.S. Geological Survey, 2025. https://pubs.usgs.gov/publication/mcs2025.
[84] RMIS - Raw Materials Information System, RMIS - raw materials' profiles, 2024. Available from: https://rmis.jrc.ec.europa.eu/rmp/Natural%20Graphite (cited 2025 Jun 28, Internet).
[85] European Commission, Communication From the Commission to the European Parliament, the Council, the European Economic and Social Committee and the Committee of the Regions on the Review of the List of Critical Raw Materials for the EU and the Implementation of the Raw Materials Initiative, European Commission, Brussels, May 2014. Available from: https://eur-lex.europa.eu/legal-content/EN/TXT/PDF/?uri=CELEX:52014DC0297 (Report No.: COM (2014) 297 Final, Internet).
[86] K. Tsuji, Global Value Chains: Graphite in Lithium-ion Batteries for Electric Vehicles, Available from: https://www.usitc.gov/publications/332/working_papers/gvc_paper.pdf, May 2022 (Report No.: Office of Industries | Working Paper ID-090, Internet).
[87] L. Masterson, Viewpoint: China overshoots on battery anodes |, Available from:, Latest Market News, 2023. https://www.argusmedia.com/en/news-and-insights/latest-market-news/2405749-viewpoint-china-overshoots-on-battery-anodes (cited 2025 Aug 4, Internet).
[88] S. Pan, Yunnan Shanshan fires up new graphite anode project amid challenging market conditions, Available from: https://www.fastmarkets.com/insights/yunnan-shanshan-fires-up-new-graphite-anode-project/, 2023 (cited 2025 Aug 4, Internet).
[89] Regulation (EU) 2024/1252 of the European Parliament and of the Council of 11 April 2024 establishing a framework for ensuring a secure and sustainable supply of critical raw materials and amending Regulations (EU) No 168/2013, (EU) 2018/858, (EU) 2018/1724 and (EU) 2019/1020 (Text with EEA relevance), Available from: http://data.europa.eu/eli/reg/2024/1252/oj/eng, Apr 11, 2024 (Internet).
[90] European Commission, COMMISSION DECISION of 25.3.2025 recognising certain critical raw material projects as Strategic Projects under Regulation (EU) 2024/1252 of the European Parliament and of the Council. Brussels, Available from: https://eur-lex.europa.eu/eli/dec/2025/840/oj/eng, March 2025 (Report No.: C (2025) 1904 final, Internet).
[91] European Commission, COMMISSION DECISION of 4.6.2025 recognising certain critical raw material projects located in third countries and in overseas countries or territories as Strategic Projects under Regulation (EU) 2024/1252 of the European Parliament and of the Council. Brussels, Available from: https://single-market-economy.ec.europa.eu/document/download/808502c2-21c7-4ca8-855f-ff0b528f91c4_en?filename=C_2025_3491_1_EN_ACT_part1_v4.pdf, June 2025 (Report No.: C(2025) 3491 final, Internet).
[92] SalromGrafit, Objectives, Available from: https://www.salromgrafit.ro/objectives.html (cited 2026 Feb 13, Internet).
[93] Vittangi, Talga Group. . Available from: https://www.talgagroup.com/our-operations/vittangi/ (cited 2026 Feb 13, Internet).
[94] J. Gronholt-Pedersen, J. Gronholt-Pedersen, Greenland approves 30-year mining permit for EU-backed graphite project, Available from:, Reuters, Dec 9 2025. https://www.reuters.com/business/energy/greenland-approves-30-year-mining-permit-eu-backed-graphite-project-2025-12-09/.
[95] Maniry Graphite Project, Madagascar, 2023. Available from: https://www.mining-technology.com/projects/maniry-graphite-project-madagascar/?utm_source=chatgpt.com&cf-view (cited 2026 Feb 13, Internet).
[96] Pearson J. BULLS N'' BEARS, Sarytogan Graphite woos $5m investment from European bank, Available from: https://www.bullsnbears.com.au/post/sarytogan-graphite-woos-5m-investment-from-european-bank, 2024 (cited 2026 Feb 13).
[97] С. Микола, BGV presented its graphite and rare earth projects at an international conference in Brussels, Available from:, BGV Graphite, 2024. https://www.bgv-graphite.com.ua/en/bgv/ (cited 2026 Feb 13, Internet).
[98] AdminBF, Tokai COBEX. France for batteries, Available from: https://francefor batteries.fr/tokai-cobex/, 2023 (cited 2026 Feb 13, Internet).
[99] UP catalyst: transforming carbon emissions into sustainable graphite, EIT. . Available from: https://www.eit.europa.eu/news-events/success-stories/catalyst-transforming-carbon-emissions-sustainable-graphite (cited 2026 Feb 13, Internet).
[100] Northern Graphite proposal for battery anode material plant in france wins EU strategic project status, Available from:, Northern Graphite, 2025. https://www.northerngraphite.com/northern-graphite-proposal-for-battery-anode-material-plant-in-france-wins-eu-strategic-project-status/ (cited 2026 Feb 13, Internet).
[101] About Hycamite, Hycamite. . Available from: https://hycamite.com/about-us/ (cited 2026 Feb 13, Internet).
[102] Ganzheitliche Bilanzierung von Brennstoffzellen in der Energie- und Verkehrstechnik. Als Ms. gedr, VDI-Verl, Düsseldorf, 2002. Available from: https://d-nb.info/964567008/04 (cited 2025 Jun 24, 238 p. (Verein Deutscher Ingenieure), Internet).
[103] Q.Q. Zhang, X.Z. Gong, X.C. Meng, Environment impact analysis of natural graphite anode material production, Mater. Sci. Forum 913 (Feb 2018) 1011–1017.
[104] S.W. Gao, X.Z. Gong, Y. Liu, Q.Q. Zhang, Energy consumption and carbon emission analysis of natural graphite anode material for lithium batteries, Mater. Sci. Forum 913 (Feb 2018) 985–990.
[105] Nouveau Monde Graphite, Life Cycle Assessment of NMG's Graphite Advanced Materials Confirm Minimal Environmental Footprint, Available from: https://nmg.com/wp-content/uploads/2022/07/CMQ-LCA-2022.07.18-vFINALE.pdf, 2022 Jul (Montréal, Canada, Internet).
[106] Canada Energy Regulator, Canada's Energy Future Data Appendices, 2024, https://doi.org/10.35002/zjr8-8x75 (cited 2025 Jun 30, Internet).
[107] Talga Group Ltd, Talga's battery anode sustainability underpins leadership position in European market, Available from: https://talgagroup.eu-central-1.linodeobjects.com/app/uploads/2023/08/09154607/20230809LCAUpdate_ASX.pdf, Aug 2023.
[108] Ecoinvent v 3.11-cutoff. coated natural graphite production - China - natural graphite, coated, ecoQuery, 2024. Available from: https://ecoquery.ecoinvent.org/3.11/cutoff (Internet).
[109] Sphera, Sphera, 2024. Available from: https://lcadatabase.sphera.com/.
[110] Ecoinvent v 3.7.1-cutoff. graphite production, battery grade - China - graphite, battery grade, ecoQuery, 2020. Available from: https://ecoquery.ecoinvent.org/3.7.1/cutoff/dataset/3576/documentation (Internet).
[111] J.B. Dunn, C. James, L. Gaines, K. Gallagher, Q. Dai, J.C. Kelly, Material and Energy Flows in the Production of Cathode and Anode Materials for Lithium Ion Batteries, Argonne National Lab. (ANL), Argonne, IL (United States), Sep 2015. Report No.: ANL/ESD-14/10 Rev. Available from: https://www.osti.gov/biblio/1224963 (cited 2025 May 18, Internet).
[112] Ecoinvent v 3.8-cutoff. synthetic graphite production, battery grade - China - synthetic graphite, battery grade, ecoQuery, 2021. Available from: https://ecoquery.ecoinvent.org/3.8/cutoff/dataset/24786/documentation (Internet).
[113] J. Daimer, 6.2 Manufacturing, in: Industrial Carbon and Graphite Materials vol. I, John Wiley & Sons, Ltd, 2021, pp. 214–229. Available from: https://onlinelibrary.wiley.com/doi/abs/10.1002/9783527674046.ch6_2 (cited 2025 Jun 25, Internet).
[114] Epsilon Advanced Materials, Epsilon advanced materials sustainability report 2023-24, Available from: https://www.epsilonam.com/pdf/EAMPL_SR_23-24_5-12-24.pdf, 2023 (cited 2025 Jun 17, Internet).
[115] Vianode, Vianode sustainability report 2024, Available from: https://vianode.fra1.digitaloceanspaces.com/documents/Vianode-Sustainability-Report-2024.pdf, 2024 (Internet).
[116] R. Pandey, U.R. Gracida-Alvarez, R.K. Iyer, J.C. Kelly, Energy, greenhouse gas, and water life cycle analysis of synthetic graphite anode production in the United States, Environ. Sci. Adv. 4 (Oct 1 2025) 2055–2068. Available from: https://pubs.rsc.org/en/content/articlelanding/2025/va/d5va00171d (cited 2025 Oct 10, Internet).
[117] Ecoinvent v 3.11-cutoff. synthetic graphite production, battery grade, via Acheson powder route - China - synthetic graphite, battery grade, ecoQuery, 2024. Available from: https://ecoquery.ecoinvent.org/3.11/cutoff/dataset/92933/documentation (Internet).
[118] M. Wang, H. Cai, L. Ou, A. Elgowainy, P.T. Benavides, L. Benvenutti, et al., Summary of Expansions and Updates in R&D GREET® 2025 (Technical Report), Argonne National Laboratory: Energy Systems and Infrastructure Assessment Division, Dec 2025. Report No.: ANL/ESIA-25/16. Available from: https://greet.anl.gov/files/greet-2025-summary (Internet).
[119] F. Cerdas, P. Titscher, N. Bognar, R. Schmuch, M. Winter, A. Kwade, et al., Exploring the effect of increased energy density on the environmental impacts of traction batteries: a comparison of energy optimized lithium-ion and lithium-sulfur batteries for mobility applications, Energies 11 (1) (Jan 2018) 150.
[120] Z. Wu, D. Kong, Comparative life cycle assessment of lithium-ion batteries with lithium metal, silicon nanowire, and graphite anodes, Clean Techn. Environ. Policy 20 (6) (Aug 1 2018) 1233–1244.
[121] B. Cox, C.L. Mutel, C. Bauer, A. Mendoza Beltran, D.P. van Vuuren, Uncertain environmental footprint of current and future battery electric vehicles, Environ. Sci. Technol. 52 (8) (Apr 17 2018) 4989–4995.
[122] J.F. Peters, M. Baumann, J.R. Binder, M. Weil, On the environmental competitiveness of sodium-ion batteries under a full life cycle perspective – a cell-chemistry specific modelling approach, Sustain. Energy Fuels 5 (24) (Dec 7 2021) 6414–6429.
[123] E. Crenna, M. Gauch, R. Widmer, P. Wäger, R. Hischier, Towards more flexibility and transparency in life cycle inventories for lithium-ion batteries, Resour. Conserv. Recycl. (170) (Jul 1 2021) 105619.
[124] J.C. Kelly, Q. Dai, M. Wang, Globally regional life cycle analysis of automotive lithium-ion nickel manganese cobalt batteries, Mitig. Adapt. Strateg. Glob. Chang. 25 (3) (Mar 1 2020) 371–396.
[125] M. Abdelbaky, L. Schwich, J. Henriques, B. Friedrich, J.R. Peeters, W. Dewulf, Global warming potential of lithium-ion battery cell production: determining influential primary and secondary raw material supply routes, Clean Logist. Supply Chain. (9) (Dec 1 2023) 100130.
[126] P. Voß, B. Gruber, M. Mitterfellner, J.D. Plöpst, F. Degen, R. Schmuch, et al., Benchmarking state-of-the-art sodium-ion battery cells – modeling energy density and carbon footprint at the gigafactory-scale, Energy Environ. Sci. (2025), https://doi.org/10.1039/D5EE00415B.
[127] J. Sprengelmeyer, M. Weil, W. Bauer, H. Ehrenberg, Sustainability assessment of sodium-ion batteries: benchmarking vs. NMC, LFP, and LMFP across value chains, Available from: https://www.batterieforum-deutschland.de/events/batterieforum-deutschland-2025/, 2025.
[128] A. Kampker, H. Heimes, C. Offermanns, S. Wennemar, T. Robben, N. Lackner, Optimizing the cell finishing process: an overview of steps, technologies, and trends, World Electr. Veh. J. 14 (4) (Apr 2023) 96.
[129] L. Yu, Y. Bai, B. Polzin, I. Belharouak, Unlocking the value of recycling scrap from Li-ion battery manufacturing: challenges and outlook, J. Power Sources (593) (Feb 15 2024) 233955.
[130] J.F. Peters, M. Weil, Providing a common base for life cycle assessments of Li-ion batteries, J. Clean. Prod. (171) (Jan 10 2018) 704–713.

[131] L. Sun, C. ping Xu, K. yan Xiao, Y. sheng Zhu, L. ya Yan, Geological characteristics, metallogenic regularities and the exploration of graphite deposits in China, China Geol. 1 (3) (Sep 1 2018) 425–434.
[132] S. Stock, J. Hagemeister, S. Grabmann, J. Kriegler, J. Keilhofer, M. Ank, et al., Cell teardown and characterization of an automotive prismatic LFP battery, Electrochim. Acta 471 (Dec 10 2023) 143341.
[133] F. Degen, M. Winter, D. Bendig, J. Tübke, Energy consumption of current and future production of lithium-ion and post lithium-ion battery cells, Nat. Energy 8 (11) (Nov 2023) 1284–1295.
[134] M. Titirici, P. Johansson, M. Crespo Ribadeneyra, H. Au, A. Innocenti, S. Passerini, et al., 2024 roadmap for sustainable batteries, J. Phys. Energy. 6 (4) (Oct 1 2024) 041502.
[135] S. Gorman, C. Hitt, S. Kesler, G. Keoleian, H.C. Kim, R. De Kleine, et al., Us graphite sourcing for electric vehicle battery applications, J. Ind. Ecol. (2025). Available from: https://onlinelibrary.wiley.com/doi/abs/10.1111/jiec.70104 (cited 2025 Oct 20, n/a(n/a), Internet).
[136] P. Dolega, M. Buchert, J. Betz, Ökologische und sozio-ökonomische Herausforderungen in BatterieLieferketten: Graphit und Lithium, Oeko-Institut, Darmstadt, Jul 2020. Available from: https://www.oeko.de/fileadmin/oekodoc/Graphit-Lithium-Oeko-Soz-Herausforderungen.pdf (cited 2025 Oct 21, Internet).
[137] Preliminary affirmative determination in the antidumping duty investigation of active anode material from the People's Republic of China, Available from: https://www.trade.gov/preliminary-affirmative-determination-antidumping-duty-investigation-active-anode-material-0, 2025.
[138] ExxonMobil, Superior graphite, superior acquisitions for synthetic graphite production, Available from: https://corporate.exxonmobil.com/news/corporate-news/superior-graphite-superior-acquisitions-for-synthetic-graphite-production, 2025 (cited 2025 Sep 18, Internet).
[139] Titan Mining Corp, Targeting to be the first commercial producer of US sourced and processed graphite, Available from: https://www.titanminingcorp.com/projects/graphite/ (cited 2025 Sep 18, Internet).
[140] EU member states target 66% renewable electricity by 2030, slightly short of the REPowerEU 69% goal, Available from:, Ember, 2023. https://ember-energy.org/latest-updates/eu-member-states-target-66-renewable-electricity-by-2030-slightly-short-of-the-repowereu-69-goal (cited 2025 Oct 20, Internet).
[141] Policies & action, Available from: https://climateactiontracker.org/countries/china/policies-action/?utm_source=chatgpt.com, 2025 (cited 2025 Oct 20, Internet).
[142] United States, Ember, 2025. Available from: https://ember-energy.org/countries-and-regions/united-states-of-america (cited 2025 Oct 20, Internet).
[143] Government of Canada SC, Hydroelectricity generation dries up amid low precipitation and record high temperatures: electricity year in review 2023, Available from: https://www.statcan.gc.ca/o1/en/plus/5776-hydroelectricity-generation-dries-amid-low-precipitation-and-record-high-temperatures, 2024 (cited 2025 Oct 20, Internet).
[144] Canada, Ember, 2025. Available from: https://ember-energy.org/countries-and-regions/canada (cited 2025 Oct 20, Internet).
[145] Electric power monthly, U.S. Energy Information Administration (EIA). . Available from: https://www.eia.gov/electricity/monthly/epm_table_grapher.php?t=epmt_1_1 (cited 2025 Oct 20, Internet).
[146] International Energy Agency, Global EV outlook 2023: catching up with climate ambitions, Available from:, OECD, 2023. https://www.oecd.org/en/publications/global-ev-outlook-2023_cbe724e8-en.html.
[147] S. Hasselwander, M. Meyer, I. Österle, Techno-economic analysis of different battery cell chemistries for the passenger vehicle market, Batteries 9 (7) (Jul 15 2023) 379.
[148] X. Han, L. Lu, Y. Zheng, X. Feng, Z. Li, J. Li, et al., A review on the key issues of the lithium ion battery degradation among the whole life cycle, eTransportation 1 (Aug 1 2019) 100005.
[149] S. Evro, A. Ajumobi, D. Mayon, O.S. Tomomewo, Navigating battery choices: a comparative study of lithium iron phosphate and nickel manganese cobalt battery technologies, Future Batter. (4) (Dec 1 2024) 100007.